INDIAN WELDING JOURNAL Volume 55 No. 4, October 2022

KEITH HARTLEY MEMORIAL AWARD LECTURE 2021

Recent Developments in Materials Joining and Welding

V. Balasubramanian
Professor & Director
Centre for Materials Joining & Research (CEMAJOR)
Faculty of Engineering & Technology
Annamalai University, Annamalainagar
(P.O), Chidambaram – 608002
Email: visvabalu@yahoo.com

ORCID: V Balasubramaniam: https://orcid.org/ 0000-0001-7658-6392

DOI : 10.22486/iwj.v55i4.217830

Abstract

Joining and welding is an essential component of manufacturing technology. New developments in joining and welding are evolved in order to acquire extraordinary benefits such as unique joint properties, synergistic mix of materials, cost reduction of component, increase productivity and quality, complex geometrical configurations, suitability and selection of material to manufacture new products. This paper provides an update on recent developments of welding and joining to showcase above benefits. Theoretical background, process parameters, novel aspects, process capabilities, and process variants along with its application are presented in this paper. The recent research works carried out in Centre for Materials Joining & Research (CEMAJOR), Annamalai University on advanced welding and joining techniques such as friction stir welding (FSW), diffusion bonding (DB), linear friction welding (LFW) , gas tungsten constricted arc welding (GTCAW), rotating arc gas metal arc welding (RAGMAW) and wire arc additive manufacturing (WAAM) are discussed in this paper.

1.0 Comparison of Performance of FSW Joints and Riveted Joints

Friction stir welding (FSW) is a solid-state welding process. It is commonly a type of friction welding but due to its versatile applications, it is considered as a separate welding process. In this type of welding process, no external heat is supplied and the joint formation takes place due to plastic deformation at the interface under high pressure and frictional force. In this process, no phase transformation involves so it is categorized into solid state welding processes works on same principle of friction welding. FSW is performed using a non-consumable tool, with a profiled probe and shoulder, is rotated and plunged into the interface between two work pieces (**Fig.1**). until the probe pierces into the workpiece and shoulder touches the surface of the workpieces. The probe is always slightly shorter than the thickness of the workpiece, with the tool shoulder riding a top the work surface. After a short dwell time, the tool is moved forward along the joint line at the pre-determined traverse speed, causing the material to heat and soften. The shoulder also acts to contain this plasticized material, which is mechanically mixed to create a solid phase weld. FSW can also eliminate all of the fusion welding problems such as hot cracking, alloy segregation, partially melted zone and porosity and reduces manufacturing complexity. Furthermore, the joints fabricated using FSW exhibited higher strength than the fusion welding process. Due to dynamic recrystallization in the weld and phase transformation is completely restricted during FSW. Hot rolled aluminum alloy of grade AA2014-T6 was chosen as base metal in this investigation. The sheet thickness was chosen as 2 mm for fabricating the joints. Preliminary test such as chemical composition and mechanical properties were carried using spark ignition method and tensile test respectively. The optical microstructure of base metal shows the presence of equiaxed grains. Computer numerical control FSW (CNC-FSW) machine with constant mode was employed in this work (**Fig.2a**). The joints were developed using a FSW tool (non-consumable) with a taper threaded probe (**Fig.2b**). The threaded probe accelerates more plasticized material and the shoulder diameter and pin diameter ratio of 3 were used. Optimized process parameters were used to fabricate both lap (Tool rotational speed of 900 rpm, welding speed of 100

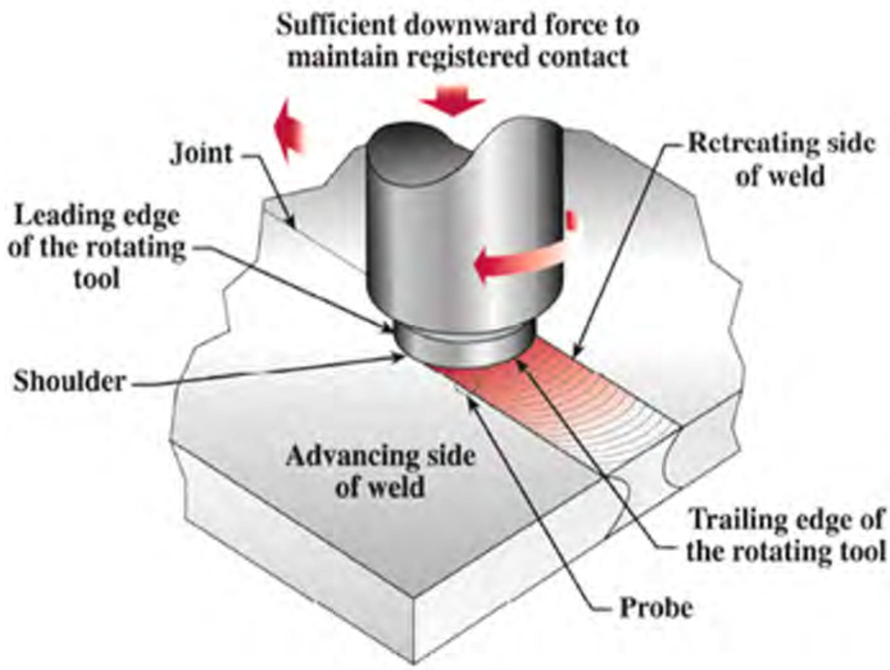

Fig. 1 : Schematic representation of FSW process

Table 1 : Strength properties of joints

Sl.No.	Joint Type	Elongation (%)	Peak Load "kN"	Microhardness "VHN"	Fracture location
1	FBJ	4.5	51.05	135	SZ / TMAZ
2	FLJ	2.3	50.20	128	SZ / TMAZ
3	SBJ	2.6	22.80	-	Along rivets
4	DBJ	4.9	40.90	-	Along rivets
5	RLJ	3.1	29.80	-	Along rivets

Fig. 2 : (a) Friction stir welding machine, (b) Fabricated FSW tools

mm/min, shoulder diameter of 12 mm and tool tilt angle of 2.0°) and butt joints (Tool rotational speed of 1500 rpm, welding speed of 50 mm/min, shoulder diameter of 6 mm and tool tilt angle of 1.5°). Similarly, the riveted joints were performed using standard shop practice (Hindustan Aeronautical Development Agency, Bangalore, India). FSW butt welded joint is mentioned to as an FBW, while FLW is denoted the lap welded joint (**Fig.3a-f**). The single cover riveted butt joint and double-cover riveted butt jointed is nomenclature as DRB and SCR respectively (**Fig.3g-l**). The joints made using rivets in butt and lap joint configuration is represented as RBJ and RLJ respectively. Composite tensile specimens were extracted from the welded specimens and tested using universal testing machine. The transverse cross-sectioned specimen was ground and polished with different grades of sandpaper and etched with Keller's reagent to revel different regions of weld.

An optical microscope with image-analysing software was employed to measure the size and orientation of grains in different regions of joints. The fractured area of tested specimens was analysed using scanning-electron-microscope. Transmission-electron-microscope was utilized to analyze the size and morphology of precipitates in weld zone. The Vickers microhardness was measured employing a load of 0.50 N and holding time of 15 seconds, evaluate the hardness distribution over the weld zone. The energy-dispersive-spectroscopy was selected to analyze elemental distribution in weld. The FLJ and FBJ joints disclosed superior load carrying capability of 50.2 kN and 51.5 kN respectively (**Table 1**). Similarly, tensile elongation was observed to be 2.3 % and 4.5 % respectively for FLJ and FBJ joints. Whereas the riveted joints DBJ and RBJ showed comparatively lower load carrying capability. The maximum load-carrying capacities of DBJ, RBJ and RLJ joints was observed to be 40.9 kN, 22.8 kN and 29.8 kN respectively.

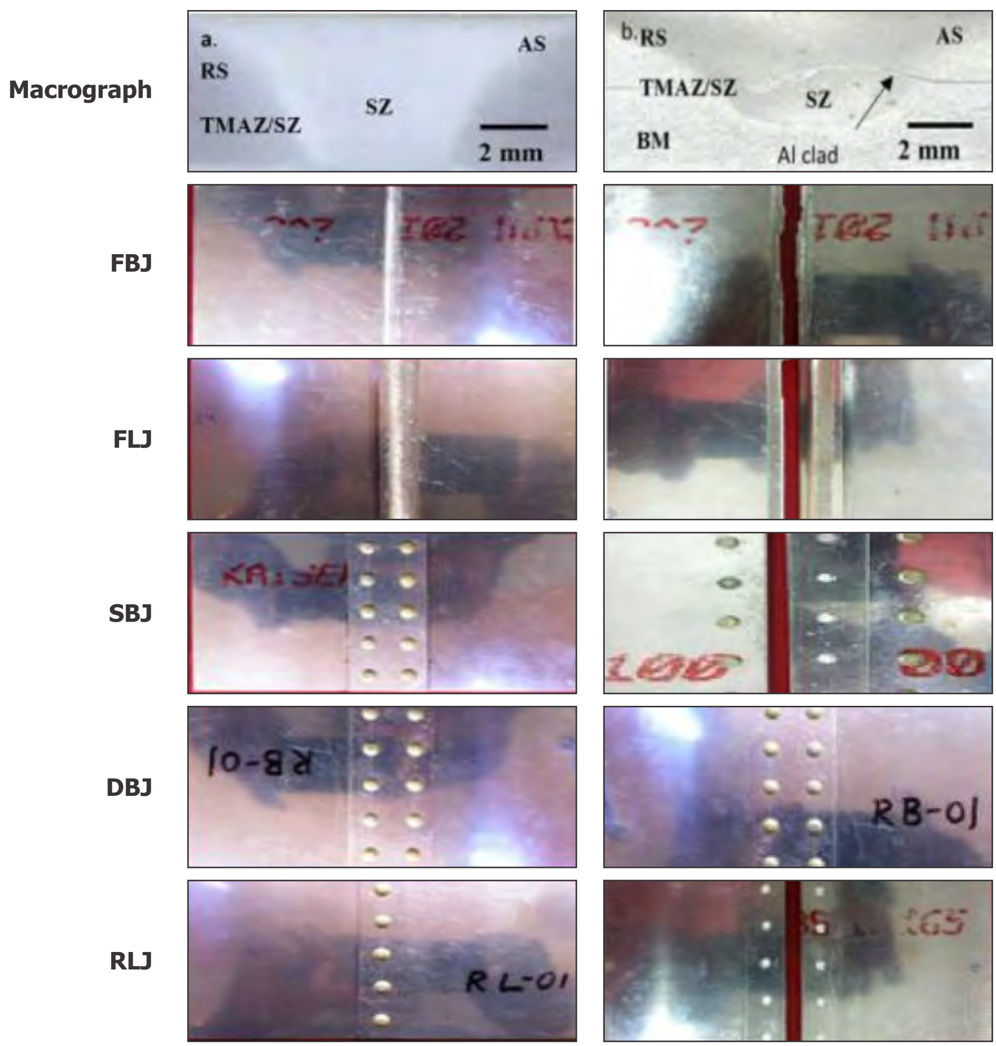

Fig. 3 : a,b) Macrograph of FBJ and FLJ, c-l) Photograph of fabricated FSW and Riveted joints (before and after fracture)

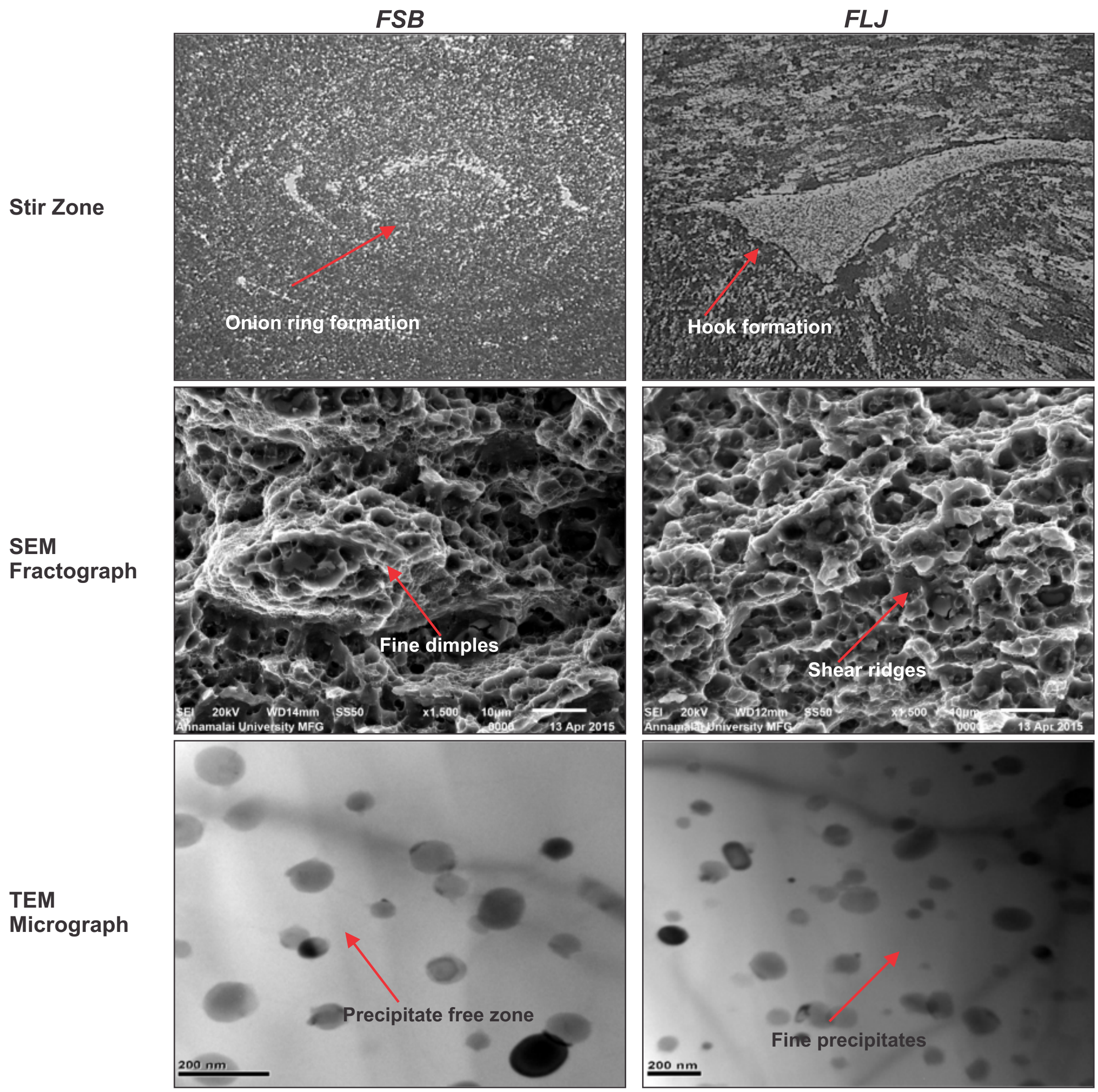

Fig.4 : Micrograph of stir zone of a,b) FBJ and FLJ, SEM fractography of c,d) FBJ and FLJ, TEM micrograph of e,f) FBJ and FLJ

The DBJ, SBJ and RLJ joints disclosed the tensile elongation of 4.9%, 2.6% and 3.1%, respectively (**Fig.3a**). The FBJ joints are capable of holding 75 % more weight than RBJ joints. Similarly, FLJ joints exhibit 70% higher load-carrying capabilities than RLJ joints. Thus, FSW offers superior strength performance than riveting in joining AA2024-T6 alloy.

In the FSW process, the sound joint depends on the following factors: pin profile, material flow, peak temperature in the stir zone, stir zone formation and hook formation in the lap joint. All the FSW joints are fabricated by the utilization of frictional heat between the tool shoulder and work piece. The localized heat generation and forging force resulted in good consolidation with the plasticized material in the solid state and the phase transformations that occur during the cool down of the weld are of the solid state. Furthermore, pin profile (a taper-threaded pin) performs a crucial function in flow across the pin because a large amount of material in FSW is extruded across the pin that is close to the pinnacle surface, wherein the deformation is further complicated because of the interaction with tool shoulder. This implies that stress rate within the stir area is essentially controlled by the way of tool pin profile and further by the process parameters such as rotational speed, welding speed, shoulder diameter and tilt angle. Hence, the pin geometry (Taper Threaded) is one of the most important parameters that influence the deformation mechanism of FSW process. The peak temperature and cooling rate, experienced at any location in the joint during FSW, are the most important factors that determine the microstructural and tensile properties of the weld because the recrystallization of AA2014 aluminium alloy takes place between 300°C and 450°C. Very fine, recrystallized grains were observed in the stir zone of both welds (FLJ and FBJ) because of the thermo-mechanical action of the tool shoulder and forging force (**Fig.4a and b**). During the FSW cycle, the entire needle-like precipitate ($CuAl_2$) and rod-shaped precipitate was dissolved in the aluminium matrix because of the peak temperature. Moreover, solid solution strengthening occurred in stir zone (**Fig.4e-f**). Because of higher precipitate dissolution and the nature of metallurgical bonding, superior mechanical properties were achieved.

Moreover, the bonding width in the FSW weld is higher than that of riveted joints. The riveted joints showed lower load-carrying capabilities in both joint configurations; this is mainly because of the absence of either mechanical bonding or metallurgical bonding between the sheets. The rivets were used to mechanically lock the sheets and there was no metallurgical bonding between the sheets. This may be the reason for the lower load carrying capabilities of riveted joints. FSW joints revealed that fine dimples and populated voids of changing size and shape needed help in disseminating through the transgranular crack area, which suggests that a large stretch zone was present at the tip of the crack because of the large fracture energy that was stored (**Fig.4 c-d**). Also, the fracture location of FSW joint during a tensile test was located in advancing the side interface (stir zone/thermo-mechanically affected zone). Moreover, the fracture location of the riveted joints was seen along the rivets because of the lower load bearing area than FSW joints. Because Rivets are creating stress concentration in the fabricated structure.

2.0 Diffusion bonding of Dissimilar Materials

Steel, nickel, titanium, and their alloys are among the most precious metallic materials used in engineering sectors, particularly in the aerospace, chemical, and power plant industries. Steel alloys, nickel-base superalloys, and titanium alloys are often utilized in aeronautical engine components due to their temperature resistance. These alloys will be formed and then joined. Several major challenges arise when combining these different material components using traditional welding procedures, including alloy segregation, hot cracking, heat-affected zone cracking, and so on. As a result, the act of joining these incompatible materials necessitates the use of a complex approach to avoid all of the difficulties associated with traditional welding. The solid-state joining procedure is the most suitable category of welding processes for the dissimilar joining of these prospective aerospace alloys. Currently, the phrase "solid-state joining" refers to a broad variety of techniques. These methods differ in terms of duration, pressure, temperature, and heat application approach. Processes that use plastic deformation at greater temperatures, such as magnetically propelled arc butt welding, friction welding, and explosive welding, have a place among the other processes. Among the several solid-state joining techniques, only the Diffusion Bonding (DB) approach binds two surfaces through interatomic diffusion and tiny deformation without distortion or detectable interface. Diffusion bonding which is a solid-state bonding technique, aids the joining of similar and dissimilar materials, mostly when their physicochemical properties change by large variation without melting and controlled macroscopic deformation. Their less structural inhomogeneities due to negligible impact of temperature inclination and slightest dimensional resilience are the key component for joint development in solid-state diffusion. Five factors that influence the DB process are temperature, bonding time, surface roughness, interfacial pressure, and environment.

Optical micrographs of the base metals are displayed in **Fig. 5. Fig. 5 a**) illustrates the presence of columnar grains along the rolling direction. Since, Ti–6Al–4V is a binary phase alloy, embedded in **Fig. 5 a**) demonstrates an equiaxed α ('α' light color) phase with an intergranular β ('β' dark color) phase. In **Fig. 5 b**) there is carbide precipitation in the ASS micrograph. A photograph of a DB machine used in this investigation is displayed in **Fig. 6**.

Dissimilar DB joints were made at a bonding pressure of 14 MPa and a holding time of 75 min, with the temperature varying between750 °C and 950 °C at an interval of 50 °C steps. Experimental runs were directed at several temperatures to find the process parameter at which virtuous quality joint can be acquired with improved mechanical properties. Lap shear and ram tensile tests at room temperature were done for the bonded specimens. The Lap Shear Strength (LSS) and Bonding Strength (BS) results in the joints are charted in **Fig. 7**. Average LSS between 140 to 151 MPa and BS between 231 to 244 MPa were achieved for the bonds fabricated at various temperatures between 750 and 950 °C, bonding pressure of 14 MPa, and holding time of 75 min. It is comprehended that LSS and BS are gradually increasing with the increase in bonding temperature. At low temperatures, around 750 °C, the LSS, and BS of the joints were 140 MPa and 231 MPa. This is the shortest result showing poor contact between bonded surfaces which is attributed to the lack of thermal excitation. The grain boundary surface rigidity and grain boundary movement are less at low temperatures which control the underlying improvement of

Table 2 : Chemical composition of base metals (wt %)

Alloy	Cr	Al	Ti	Fe	Mn	Si	Ni	P	V	S
Ti-64	-	6	Bal	-	-	-	-	-	4	-
AISI 304	20	-	-	Bal	2	1	10	0.045	-	0.03

Table 3 : Mechanical properties of base metals

Alloy	0.2% Yield Strength (MPa)	Ultimate Tensile Strength (MPa)	% of Elongation
Ti-6Al-4V	880	950	14
AISI 304	215	505	30

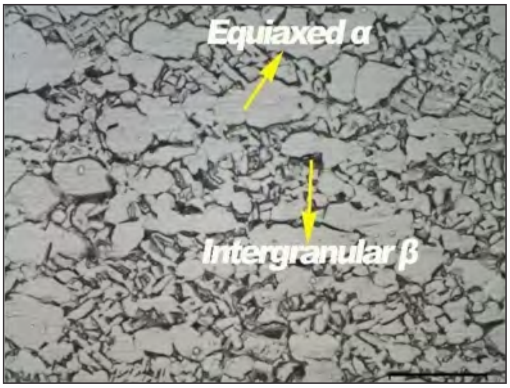

(a) Ti-6Al-4V

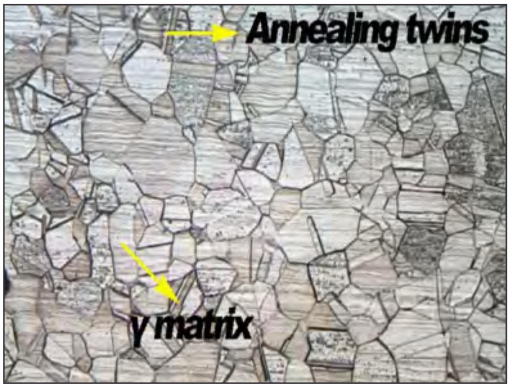

(b) AISI 304

Fig.5 : Optical micrographs of the base materials

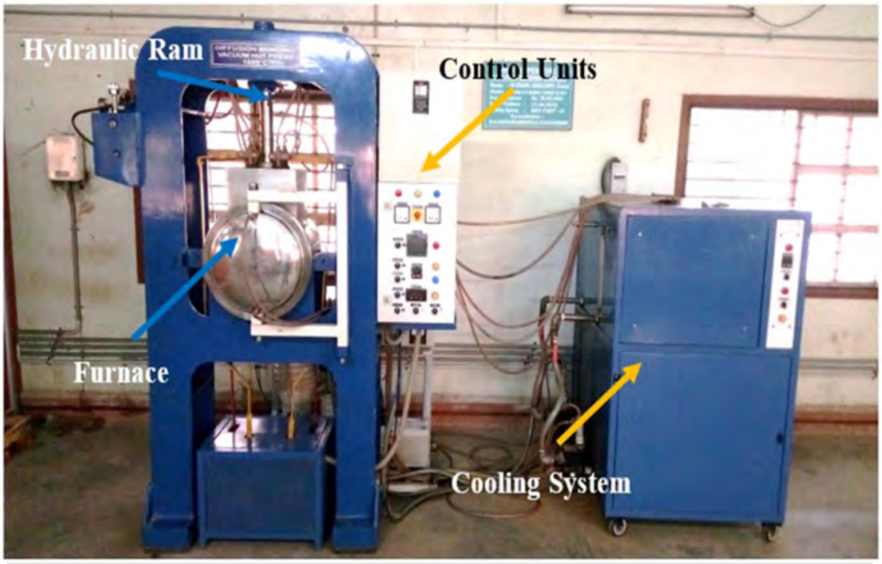

Fig.6 : Photograph of the diffusion bonding machine used for this investigation

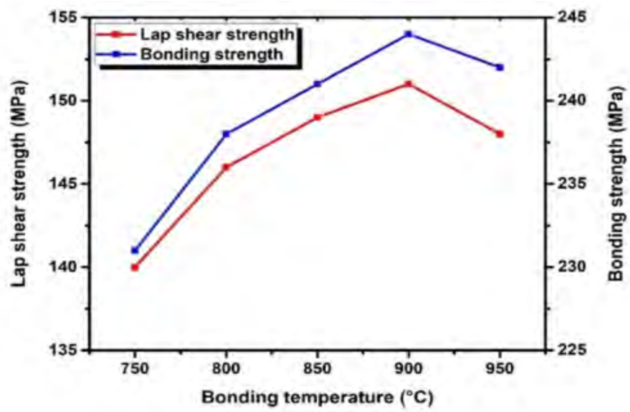

Fig. 7 : Effect of bonding temperature on joint strength

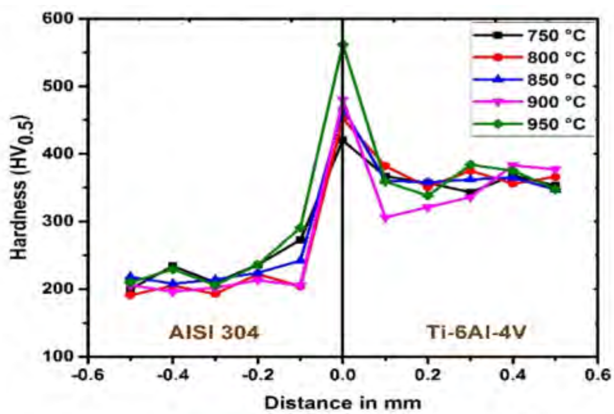

Fig. 8 : Effect of bonding temperature on microhardness

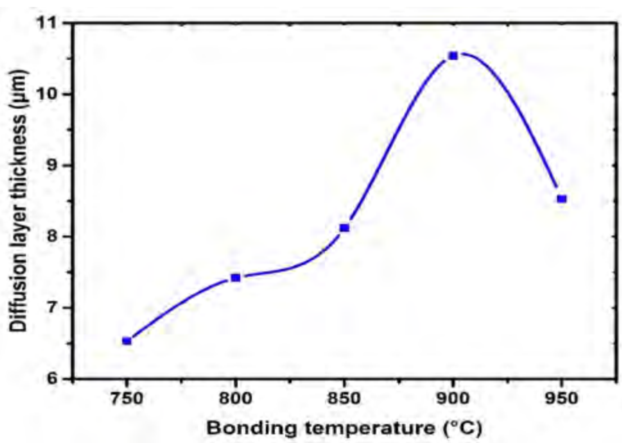

Fig. 9 : Effect of bonding temperature on the diffusion layer thickness

grain interface boundaries. At a point, when the temperature touches 900 °C, maximum LSS of 151 MPa and BS of 244 MPa were found, which results in an extensive change in LSS and BS. At higher temperatures, the contact ratio is improved, on the grounds, that the atom diffusion is higher with a higher temperature which prompts effective bonding. An additional increase in temperature to 950 °C prompts a drop-in strength due toa rise in temperature and a large advancement of mass transfer of alloying components over the interface, which is accountable for the expansion in volume fraction of the response products. The higher rate of diffusion causes the formation of a higher volume of intermetallics, an increment in joint brittleness, and a reduction in joint strength.

The microhardness values of the bonds were estimated by applying a 500 g load in the transverse path to the bonded specimens. The dissemination of the hardness values of the specimens on whichever side of the centerline appears as a graphical plot in Fig.8. It is seen that the titanium sides have high hardness values in the range of 350-380 HV, while the stainless steel sides have lower hardness values in the range of 230–320 HV. Hardness at the interface was measured and found to be in the range of 440–500 HV. The hardness values were low for a bonding temperature of 750 °C and hardness was seen to increase with increasing bonding temperature to a maximum value for a bonding temperature of 950 °C. The gradual isothermal solidification of the joint with increasing bonding temperature and the corresponding segregation of intermetallics towards the center of the joint due to the solid/liquid interface pushing these particles was thought to be the main cause for an increase in the hardness values.

In Fig. 9 average diffusion layer thickness (DLT) between 6.53 to 10.53 μm was achieved at various bonding temperatures. The ideal thickness of DL of 10.54 μm was achieved at 900 °C. When the bonding temperature is mulled over, it is observed that the DLT depends mostly on DB temperature. The DLT at 750 °C is 6.53 μm and it increments bit by bit by expanding the bonding temperature. When the bonding temperature reaches 900 °C, the DLT achieves the maximum; and the layer thickness relies upon atom diffusion. When the temperature for bonding increases to more than 950 °C, the DLT decreases and the bonding process permits the elements of both the metals to diffuse and promotes the different chemical phases to control the weld or the DLT microstructure and the corresponding mechanical properties. An optimum DLT of 10.54 μm (formed at a bonding temperature of 900 °C) yielded better mechanical properties compared to other layer thicknesses.

Optical microscopic examination **(Fig. 10**) shows that the diffusion zone of the Ti–SS couple is separated into four regions away from each other from the existence of parent material. The bond line is free from discontinuities. The bond layer can be observed with a sound joint near the zone. The top side (region I) indicates the austenite phase of 304 SS, containing annealing twins. The heavily etched band II consists of layers of intermetallic phases containing the original interface. The Fe, Cr, and V are strong β-stabilizers of Ti. The migration of Fe, Ni, and Cr from 304 SS to the Ti alloy and the presence of V in region III retain the high-temperature BCC

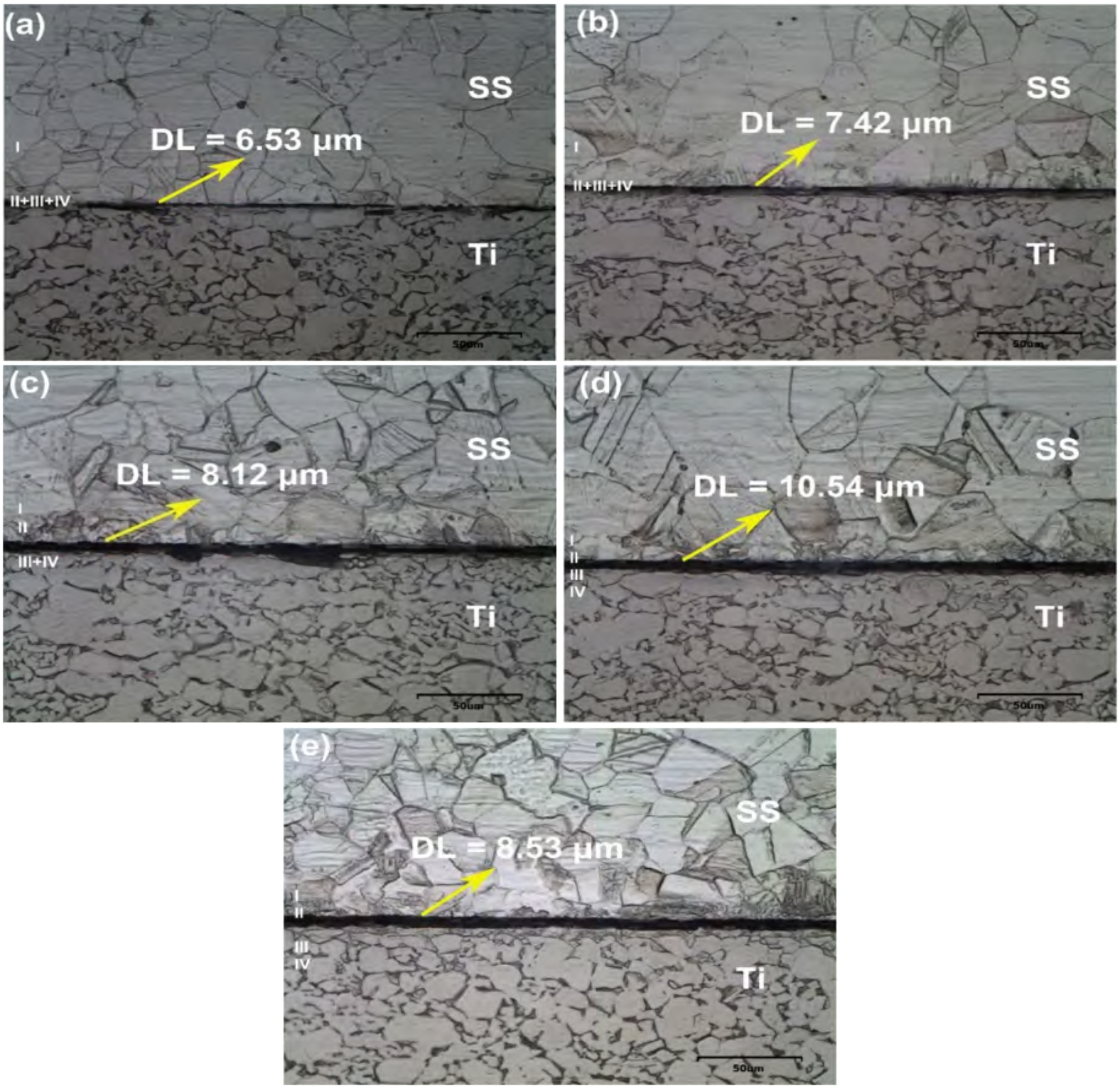

Fig. 10 Optical micrographs of the joint interface at bonding temperature of (a) 750 °C, (b) 800 °C, (c) 850 °C, (d) 900 °C and (e) 950 °C

phase of the Ti alloy at ambient temperature; hence, zone III is designated as stabilized β-Ti. Region IV consists of β-Ti with transformed α-Ti. A substantial quantity of Fe, Cr, Ni, and V in this area promotes a eutectoid transformation of the Ti alloy and, thus, the Widmanstatten morphology is developed, in which a bright β-Ti phase is embedded in the shaded α-Ti matrix. At low processing temperatures such as 750 °C, 800 °C and 850 °C zones II through IV have not been resolved clearly due to their finer width (**Fig. 10 and c**).

Fig. 7 shows the SEM and EDS results of DB samples at a bonding temperature of 900 °C, bonding pressure of 14 MPa, and holding time of 75 min. The shear fracture of the Ti6Al4V/AISI304 joint has appearances of cleavage fracture by SEM observation (**Fig. 11 a**). In addition, there are a lot of fine river patterns and quasi-cleavage fractures with a local tear (**Fig. 11 b**). This shows that the fracture of the Ti6Al4V/AISI304 joint isn't fully brittle and also seems to be a little tough. The position where the shear fracture happens relies upon interface structure in the diffusion zone.

XRD analysis was performed on the fracture surfaces after accomplishing the shear test, as it is furnished in **Fig. 8**. Energy dispersive spectrum (EDS) investigation was taken at the interface and the obtained results are exhibited in **Fig. 12** (a and b). The interface contains 49.74% of Ti and 28.77 % of iron, 9.5 % of chromium, 7.33 % aluminium, 2.5 % of vanadium, and 2.28 % of nickel. XRD analysis was performed

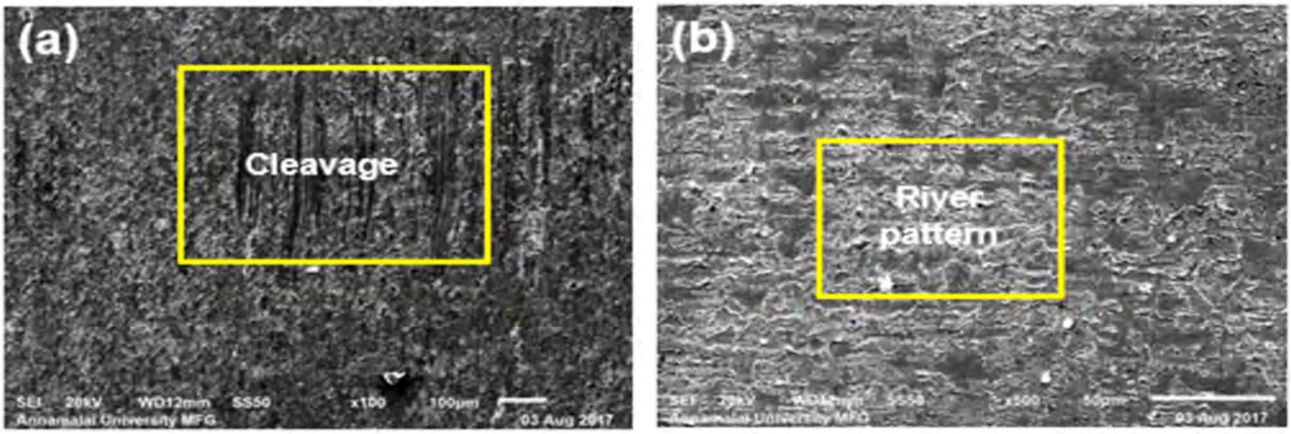

Fig. 11 : Fracture surface of the specimens (a) Ti side and (b) SS side

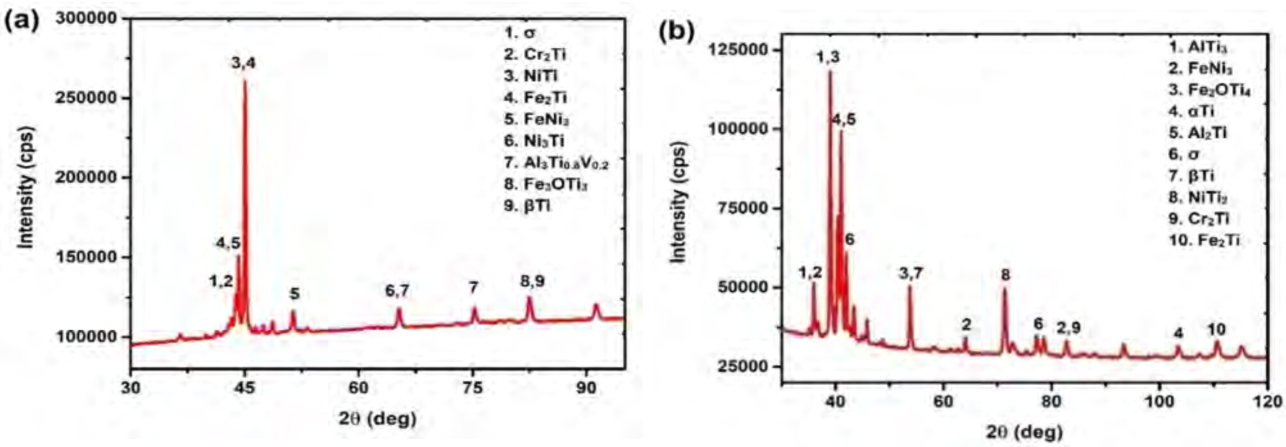

Fig. 12 : XRD pattern of fracture surfaces of (a) Ti side and (b) SS side joint bonded at 900 °C

in the interface and the obtained results are exhibited in **Fig. 13 c**.

3.0 Linear Friction Welding of Titanium Alloys

Linear friction welding (LFW) is a solid-state joining process in which a joint between two metals can be formed through the intimate contact of a plasticised layer at the interface of the adjoining specimens. This plasticised layer is created through a combination of frictional heating, which occurs as a result of pushing a stationary work piece against one that is moving in a linear reciprocating manner, and applied force. The process is currently established as a niche technology for the fabrication of titanium alloy bladed disc (blisk) assemblies in aero engines, and is being developed for nickel-based super alloy assemblies. The LFW process has four distinct phases, which are 1) Initial phase, 2) Transition phase, 3) Equilibrium phase and 4) Forging phase. During the initial phase, the parts are forced together and heat is generated through friction. The rubbing together of parts causes asperities to wear down and flatten so that the true are of the contact increases towards 100%. Fig. 14 shows LFW machine. A small amount of part shortening occurs due to the wear particle expulsion. In the transition phase, the temperature at the interface rises and therefore the strength of the material at the interface decreases. The applied load can then cause this low strength material to soften and plastically deform. At the equilibrium phase the hot plasticised material at the interface is expelled as flash, with the help of the oscillatory motion and applied pressure. During the forging phase, amplitude of oscillation is decayed to zero over a predetermined time to ensure a good alignment a forge force is rapidly applied and held for a set time to consolidate the joint.This present study deals with the mechanical and metallurgical characteristics of Linear friction welded Titanium alloy joints.

A rolled 6 mm thick plates of Ti-6Al-4V titanium alloy were used as the base material in this investigation. Two weld specimen

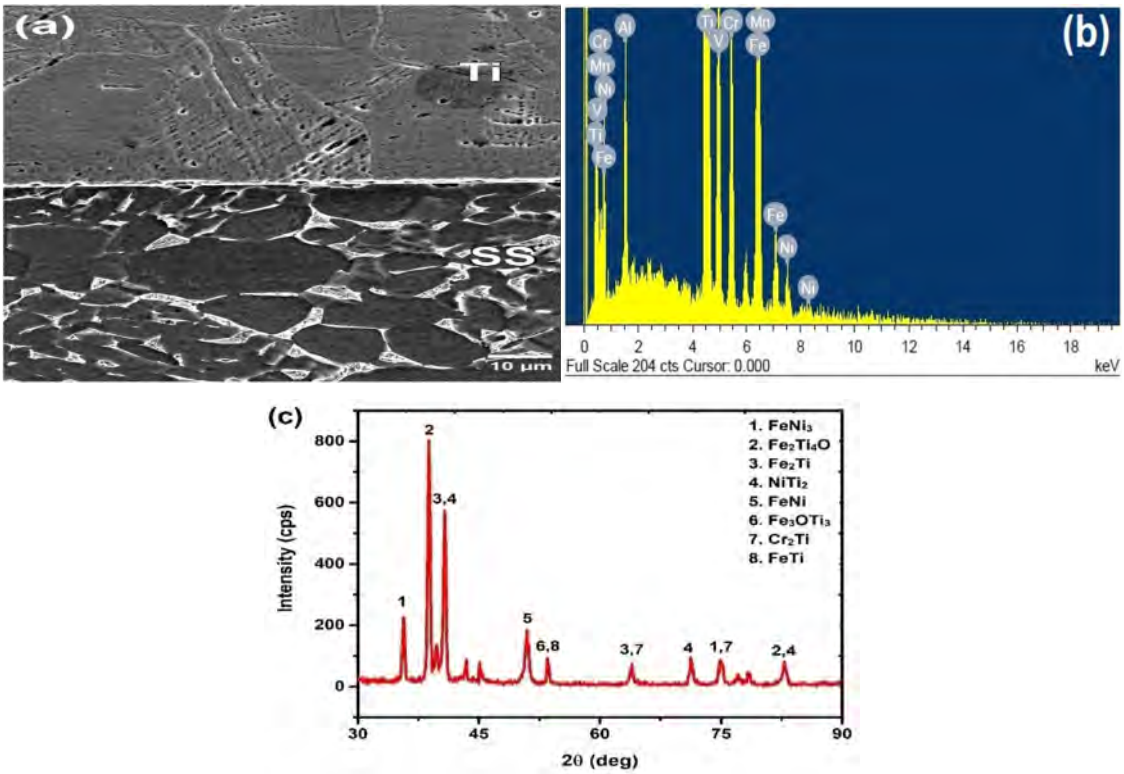

Fig. 13 : SEM with EDS analysis of diffusion bonded joint in interface processed for 75 min using 14 MPa pressing load at 900 °C (a) SEM micrograph, (b) EDS result, and (c) XRD result

dimensions 40x70 mm and 30x60 mm were used in this investigation. These two specimens were butt welded using the LFW process. The process parameters used to make the weld are mentioned in **Table 3**. **Table 4** and **Table 5** show the mechanical characteristics and chemical composition of base metal. The tensile properties, microhardness, and microstructural characteristics were evaluated for both weld joint and base metal as per ASTM standards.

Table 3 : LFW parameters

Oscillating frequency (Hz)	Friction Pressure (MPa)	Friction time (sec)	Forging Pressure (MPa)	Forging time (sec)
14	20	40	10	3

Fig.14 : Photograph of LFW Machine used for this investigation (a) Full View (b) Close-up View

Table 4 : Mechanical properties of the base metal

S.No	0.2 % Yield strength (MPa)	Ultimate tensile (MPa)	Elongation in 25 mm GL (%)	Reduction in cross-sectional area (%)	Average hardness (HV)
Ti-6Al-4V	980	1030	12	24	340

Table 5 : Chemical composition of Base Metal

Elements (wt %)	Al	V	Fe	O	C	N	H	Ti
Ti-6Al-4V	6.023	4.107	0.19	0.15	0.06	0.04	0.01	Bal.

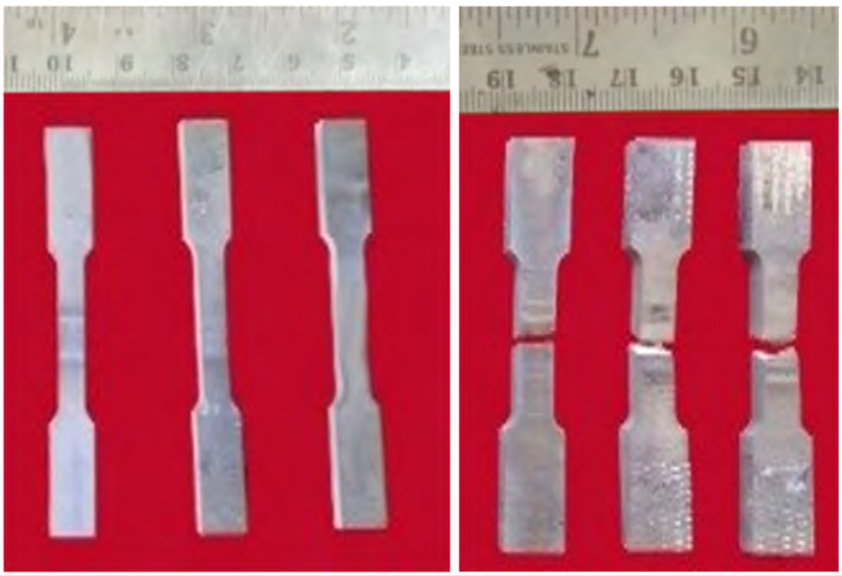

Fig.15 : Tensile specimens before and after test

Fig. 15 shows the tensile specimen before and after tensile testing. The ultimate tensile strength of the titanium alloy joint is 1015 MPa with a yield strength of 934 MPa (presented in **table 6**). The tensile specimen fractured at the intersection of TMAZ and HAZ region. This supports the lowest micro hardness value observed in that region.

Table 6 : Mechanical properties of LFW Welded Joint

Material	0.2% Yield Strength [MPa]	Ultimate Tensile Strength [MPa]	Elongation in 25 mm gauge length (%)	Reduction in cross-sectional area (%)	Joint efficiency (%)	Microhardness (HV)
Ti-6Al-4V	934	1015	13	30	98	440

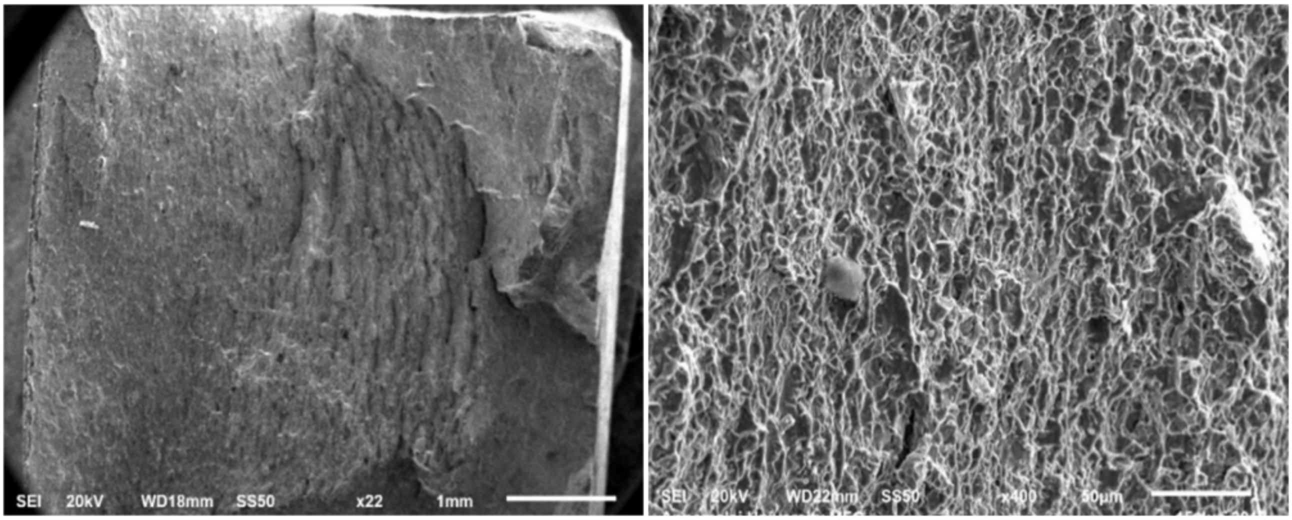

(a) Lower Magnification

(b) Higher Magnification

Fig. 16 : Fractography of Tensile Specimen

The tensile specimen fractured in a ductile mode of failure with a joint efficiency of 98%. And the strength of the weld joint is higher than the base metal as we can conclude from the hardness value of 440 HV in the weld center zone (WCZ).

3.1.1. Facture surface analysis

The fracture surfaces of tensile specimens are shown in Fig. 16 a. Tensile specimen Fractured in the interface of the TMAZ and HAZ region. The large number of fine dimples is observed in the higher magnification of fractography (**Fig. 16b**). So, the mode of failure is ductile mode of failure.

The microhardness survey carried out across the weld is also depicted in **Fig. 17** along the macrograph of the joint specimen. From the figure, it is observed that the failure location is between TMAZ and HAZ interface region which is having the lowest hardness region. The peak hardness of the joint is recorded in the weld center zone with a microhardness of 440 HV and lowest hardness of 320 HV.

The hardness of the weld center zone is the highest due to the martensite formation in the weld joint. with the lowest hardness is due to the elongated alpha and beta microstructure observed in the Fig. 18 c.

The microstructural characteristics of linear friction welded joint, using Scanning Electron Microscopy (SEM) is displayed in **Figure 4**. As compared to the base material, the structure in the central weld region of the linear friction welded Ti-6Al-4V was considerably different; the initial bimodal α-β micro-structure **(Fig. 18 a)** was transformed to martensite (α') Widmanstatten structure in the WCZ whose boundaries were

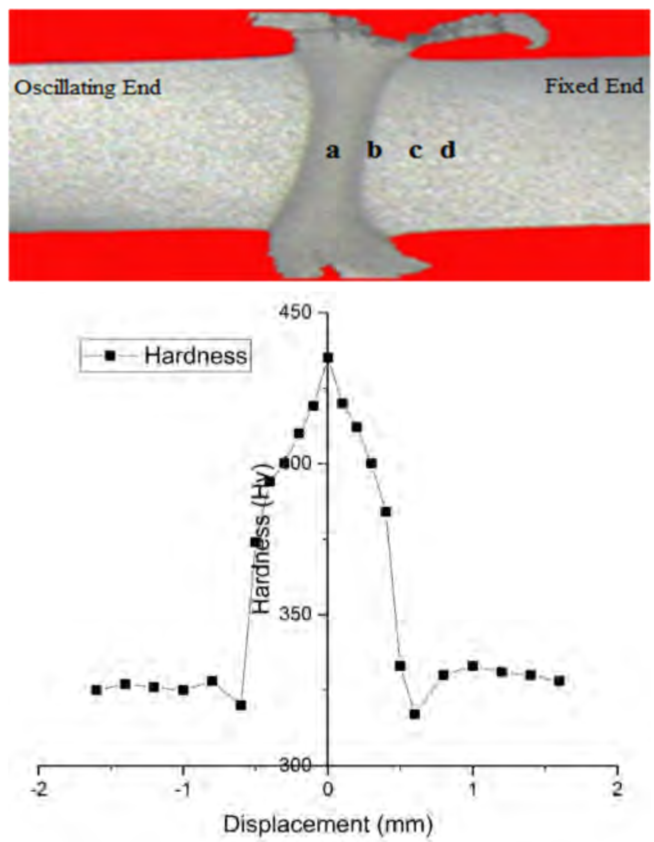

Fig. 17 : Microhardness survey across the welded joint

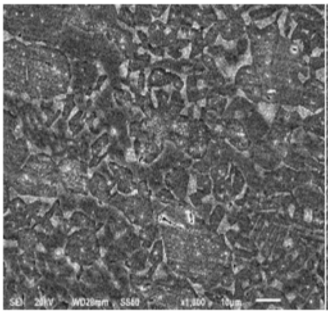

a) Base metal

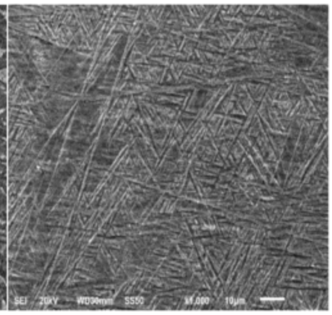

b) WCZ

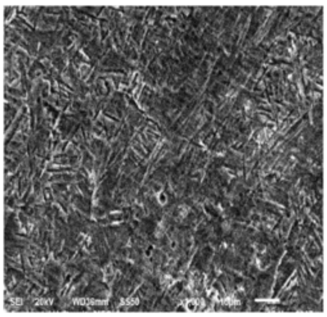

c) TMAZ

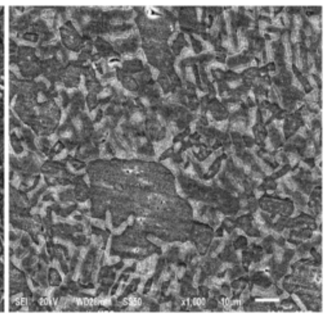

d) HAZ

Fig. 18 : Scanning Electron Microscopy of Various regions

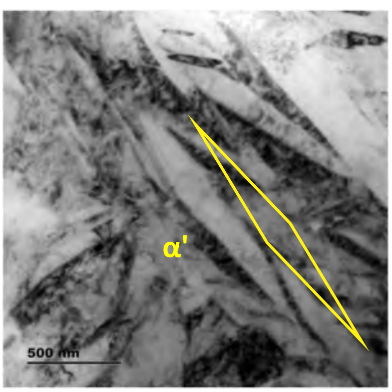

(a) WCZ

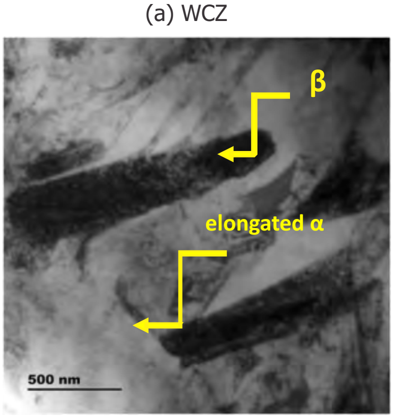

(a) TMAZ

Fig. 19 : TEM Micrograph of FDZ and TMAZ

delineated by prior-beta grains (**Fig. 18 b**). For the α–β Ti-6Al-4V alloy, this evolution in the microstructure can be justified by considering the nominal β-transition temperature of 995 °C, which represents the condition for the transformation of the microstructure to the single-phase beta field. The heat input generated during the linear friction welding, raised the temperature at the proximity of the weld interface to above the β-transus temperature, resulted in a progressive transformation of alpha to beta. At the weld center, where the temperature was the highest, implies the complete transformation of the alpha grains to prior-beta grain. In the TMAZ region **Fig. 18c** severely deformed due to the heat generated in the weld center zone, grain growth takes place in the TMAZ region. Due to the grain growth in the TMAZ region tensile specimen failure occurred in the TMAZ region. In Figure 4 (d) Heat Affected Zone (HAZ) of the weld joint can be observed, it can be seen that the microstructure in the HAZ is similar to the base metal. There are no significant changes in the microstructure of HAZ region which shows the bimodal microstructure of unaffected base material.

TEM Microstructure examination of the WCZ of the joint **Fig. 19 (a)** shows a clear picture of recrystallized super fine martensite microstructure. The fine recrystallized grain formation is due to the joined effect of shear stress, axial pressure, and frictional heat. In **Fig. 19 (b)** the large grain formation in the TMAZ is due to excessive grain growth. The grain growth rate increased due to the excessive soaking temperature maintained at the weld joint.

The maximum tensile strength and microhardness obtained is 1015 MPa and 440 HV, respectively. The corresponding parameters which yield this maximum strength were friction pressure (20 MPa), forging pressure (10 MPa), friction time (40 s), Friction time (3 s) and Frequency (14 Hz). Both the tensile specimens were failed in TMAZ region with marginal variation in toughness. The strength is higher and the fracture surface consists of finer dimples in the fractured region, so we conclude that it is ductile mode of fracture. The size of the dimples is a measure of strength and toughness. The joint fabricated using the optimized parameter shows marginally elongated dimples. The failure location was found between the TMAZ and HAZ interface region which can be attributed to the lowest hardness value (320 HV) of this region. The strength of the weld joint was stronger than the base metal for all the testing conditions.

4.0 Gas Tungsten Constricted Arc Welding of Inconel 718 Alloy

Inconel 718 is a nickel-based superalloy specifically used in high temperature aerospace applications where high strength, excellent creep and stress rupture properties, good corrosion and oxidation resistance up to 650°C are major requirements.

It accounts for 50% of the weight of gas turbine engines, being the main component for discs, blades, casings, stators and rotors of the turbine section and combustor. It is strengthened mainly by the precipitation of gamma prime [γ'- $Ni_3(Al, Ti)$] and gamma double prime [γ''- Ni_3Nb] precipitates. It exhibits excellent weldability than other nickel-based superalloys and can be welded in both solution annealed and aged conditions. It shows excellent resistance to strain age cracking due to its sluggish precipitation kinetics of gamma double prime, γ''- Ni_3Nb precipitates.

This alloy is mostly joined by gas tungsten arc welding (GTAW) process for clean, precise and high-quality joints. Also, it is economical, shop friendly and can be used for on-site fabrication or service repairing works. However, it has certain drawbacks such as high heat input and lower arc penetration due to the lower energy density associated with wider bell-shaped arc column. It leads to some metallurgical problems in welding Inconel of 718 alloy such as Nb segregation and Laves phase formation in fusion zone. The Laves phase is a brittle intermetallic compound with topologically closed packed (TCP) structure and is detrimental to the mechanical properties of welded joints. It provides low energy fracture path for crack initiation and propagation which leads to the premature failure of welded aeroengine components and increases the cost associated with component replacement. It is also more susceptible to solidification cracking and liquation cracking in heat affected zone (HAZ) due to the formation of low melting point eutectics (γ/NbC and γ/Laves) at the grain boundaries. Moreover, the joining of thin sheets of Inconel 718 alloy is more challenging to attain good weld without any defects of undercuts, porosity, penetration and distortion.

To overcome these problems, a recently emerged **Gas Tungsten Constricted Arc Welding (GTCAW)** process commercially known as Inter Pulsed TIG welding is employed to join Inconel 718 alloy sheets. It is the advanced variant of GTAW process developed by VBC Instruments Engineering, UK in association with Sheffield University to attain high quality welds with narrower bead and HAZ. It is principally differentiated by magnetic arc constriction and high frequency pulsing of welding arc up to 20 kHz. In GTCAW, the arc constriction current (known as delta current) is superimposed on main current to produce a magnetic field and constrict the arc. It pulses with main current in saw tooth shape wave form rather than square wave form in pulsed current GTAW (PC-GTAW).

The wider bell-shaped arc column in conventional GTAW results in lower energy density and requires more heat input to attain full penetration. The magnetic constriction of arc minimizes the dissipation of heat input on outer flare and causes localized fusion of metal at the joint. The magnetically constricted conical arc column enables the concentration of heat input over a narrow region. This results in large number of

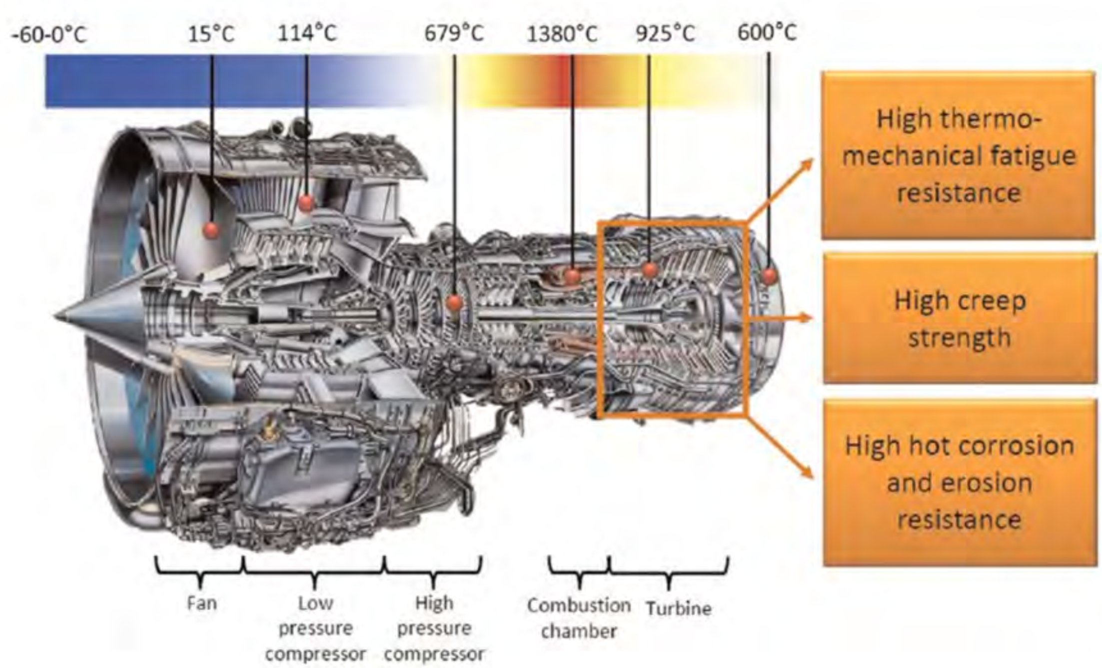

Fig. 20 : High temperature sections of gas turbine engine

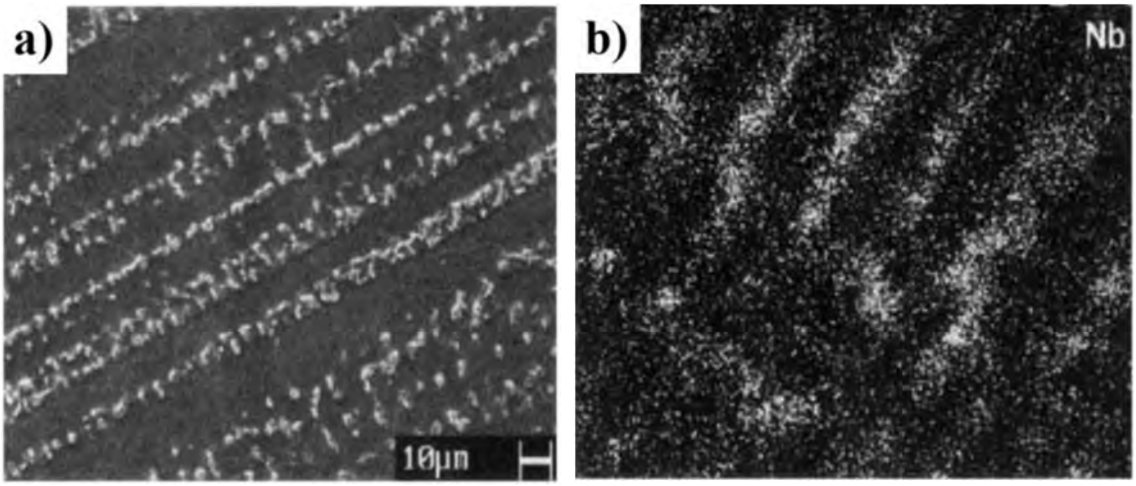

Fig. 21 : a) Coarse and Interconnected Laves phase in as weld fusion zone of Inconel 718 GTAW welds and b) X-ray Nb mapping of fusion zone showing segregation effect

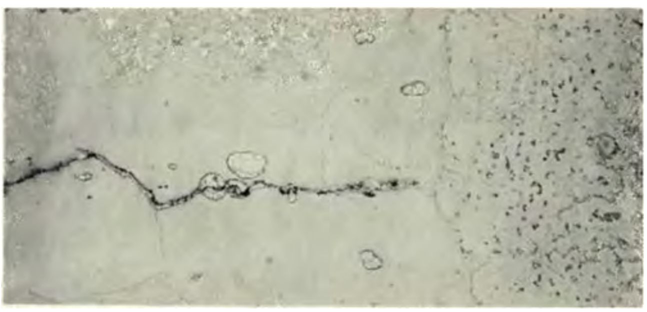

Fig. 22 : Micro fissuring in HAZ of GTA Inconel 718 welds (1000X)

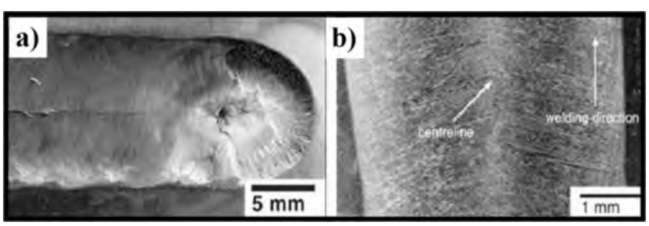

Fig.23 : Solidification cracking following autogeneous GTA welding of IN718 sheet b) Centerline grain boundary formation in IN718 sheet

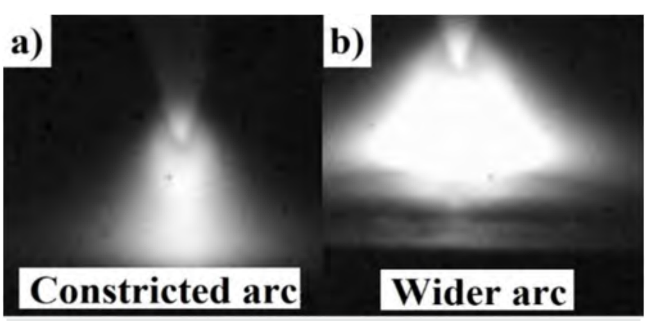

Fig. 24 : Typical welding arc in a) GTCAW and b) GTAW process

electrons striking the workpiece per unit area. The constricted arc column also minimizes the loss of heat input to the atmosphere due to the comparatively smaller surface area of arc column. Thus, there is a requirement of low heat input to attain full penetration in GTCAW process compared to conventional GTAW.

The main objective of this study is to investigate the effect of GTCAW process on weld bead geometry, microstructural features and tensile properties of Inconel 718 alloy joints for its feasibility in aerospace applications. It involves the use of arc constriction technique to reduce the segregation of Nb and Laves phase formation in Inconel 718 alloy welds for improved joint performance. The single pass autogeneous butt joints were fabricated using cold rolled thin sheets of Inconel 718 alloy (2.0 mm thick). The direct effect of GTCAW parameters on the weld bead geometry, microstructural evolution and tensile properties of welded joints was studied using one factor at a time approach of design of experiments (DoE). The performance of GTCAW joints was compared with EBW and LBW joints from literature.

Results showed that main current and welding speed being the fundamental welding parameters, showed predominant effect on the weld bead geometry, tensile properties and microstructural characteristics of Inconel 718 alloy joints followed by delta current and frequency. The joints developed using the main current of 65 A, delta current of 50 A, delta current frequency of 4 kHz and welding speed of 60 mm/min showed narrower weld bead geometry, complete joint penetration and superior tensile properties. The joints welded using optimized condition showed maximum tensile strength of 863 MPa, yield strength of 548 MPa and elongation of 27.93%. It is attributed to the microstructural refinement in fusion zone leading to the evolution of finer discrete Laves phase in interdendritic areas.

Table 7 : Tensile properties of base metal and optimized welded joint

Condition	Tensile strength (MPa)	0.2% Yield strength (MPa)	Elongation in 50 mm gauge length (%)	Joint efficiency (%)	Notch tensile strength (MPa)	Notch strength ratio (NSR)	Failure location
Base metal	870	580	38	100	805	0.92	--
Welded joint	863	548	27.93	99.42	809	0.94	FZ

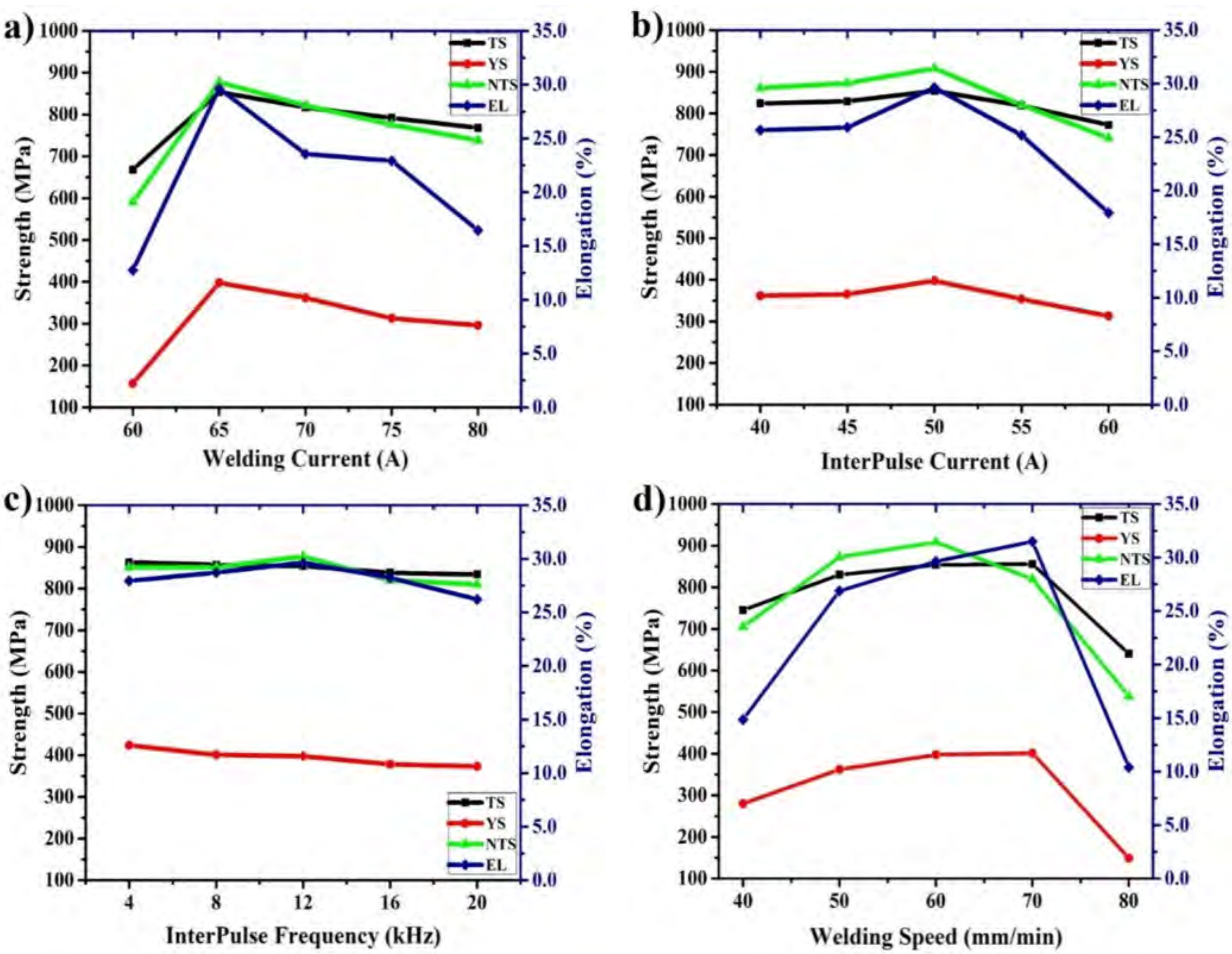

Fig. 25 : Effect of GTCAW parameters on tensile propeties of joints:
a) welding current; b) delta current; c) delta current frequency and d) welding speed

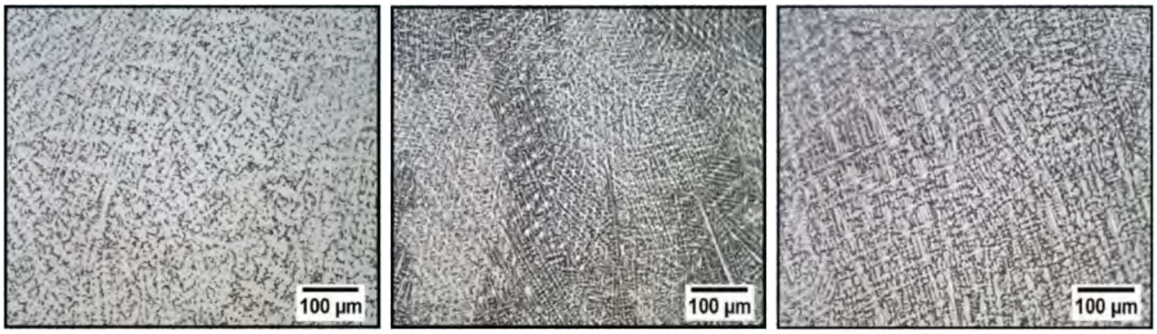

(a) 40 A (b) 50 A (c) 60 A

Fig. 26 : Effect of delta current on microstructure of fusion zone

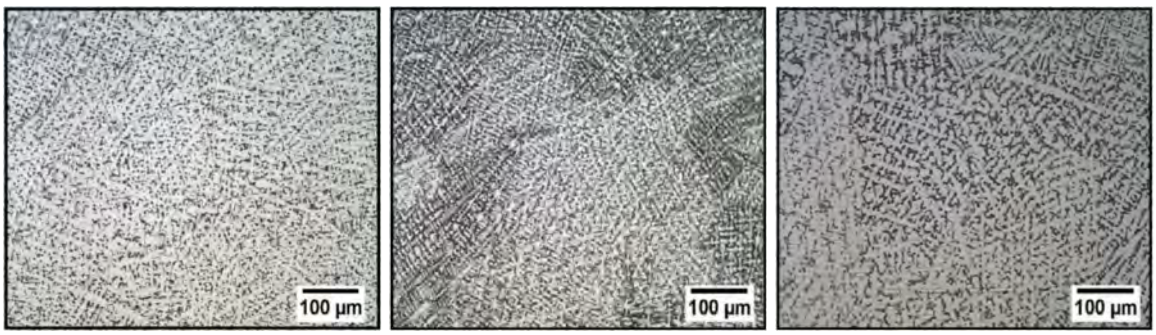

(a) 4 kHz (b) 12 kHz (c) 20 kHz

Fig. 27 : Effect of delta current frequency on microstructure of fusion zone

Table 8 : Effect of welding processes on joint efficiency of welded joints

Process	Joint efficiency (%)	Laves phase (%)
Conventional Gas Tungsten Arc Welding	71	26
Gas Tungsten Constricted Arc Welding	99.20	5.24
Electron Beam Welding	99.66	4
Laser Beam Welding	96.54	5.2

Increased levels of welding current showed drastic reduction in tensile properties and hardness of welded joints. It is attributed to the increased heat input which leads to severe grain growth in fusion zone and the evolution of lave phase in coarser and networked form. Delta current showed grain refinement and increase in tensile properties of joints up to 50 A. Further increase in delta current leads to drastic reduction in tensile properties and hardness of welded joints. It is correlated to the increased heat input associated with rise in magnetic field at constant levels of welding speed causing more localized fusion of metal at the joint and coarse lave phase evolution in fusion zone. Increase in delta current frequency (DCF) disclosed reduction in tensile properties and hardness of joints due to the coarsening of fusion zone microstructure and increased Laves phase formation in interdendritic regions. It is attributed to the stacking of heat input in weld thermal cycles at incremental levels of DCF. Increase in welding speed showed grain refinement in fusion zone microstructure due to the enhanced cooling rate leading to the lower Laves phase formation in interdendritic regions. The tensile properties increase up to 70 mm/min. Further increase in welding speed leads to drastic reduction in tensile properties of welded joints owing to the defect of incomplete penetration.

The grain refinement in fusion zone is attributed to the magnetic arc constriction and high frequency pulsing of delta current which reduces the heat input and enhances the cooling rate along with fragmentation of dendrites for the promotion of heterogeneous nucleation in fusion zone. However, the benefits of magnetic arc constriction and delta current pulsing were not achieved at higher heat input. The metallurgical problems of Nb segregation and Laves phase formation in Inconel 718 alloy welds were reduced remarkably. It showed 50-80% reduction in volume fraction of Laves phase over the results reported in literature for GTAW joints. The performance of GTCAW joints is 30% superior than conventional GTAW process and comparable to costly EBW and LBW process. Thus, proving it as a feasible solution for the fabrication and service repair works in gas turbine engine applications.

5.0 Rotating Arc Gas Metal Arc Welding (RAGMAW) of HSLA Steel

The high-strength low alloy (HSLA) steels are mostly used in shipbuilding, pipeline, and structural applications. Because these steels are having higher strength (>540 MPa), highest impact toughness (>200 J), and superior corrosion resistance. The HSLA steel microstructure mostly consists of fine pearlite mixed with high volume percentage of polygonal ferrite matrix. Currently, HSLA steels are welded by shield metal arc welding (SMAW), gas metal arc welding (GMAW), flux core arc welding (FCAW), and submerged arc welding (SAW) processes. The above-mentioned welding processes have some problems before and after welding, such as sagging defects, higher heat input, wider heat-affected zone (HAZ) softening, and lower productivity. Generally, the high thickness steel plates (>10 mm) are needed a "V" groove joint configuration for conventional arc welding processes. This type of joint configuration increases machining cost and filler metal cost; moreover, the narrow gap between SAW welding and ESW process has a higher heat input process. So, in the HAZ region, mechanical properties are deteriorated due to the development of coarse grains. Sagging of weld pool occurs due to the gravitational force that acts on the pool; it will create a sagging defect in higher thickness narrow gap welded joints.

The above mentioned problems could be overthrown by a new emerging welding technique called "SPIN ARC" welding. A customized torch is used for spin arc welding process. The torch works with both constant voltage GMAW and pulsed GMAW power sources. The main parameters affecting the process in the rotation arc welding technique are: (i) Arc rotational speed, (ii) Diameter of arc rotational, and (iii) Arc rotating direction. All these parameters can be precisely controlled using a control box included with the welding power source. Generally, spin arc welding process is developed to reduce the heat input, improve sidewall fusion, increase productivity by eliminating edge preparation and reduce the number of passes without any compromise on strength properties in weld joints. In this process, the filler wire was rotated by a special type of rotating motor within itself. This rotating filler wire will rotate the arc between the welding plates. During welding, the rotation arc should be rotated in a circular motion, so it creates the centrifugal force on the arc. This force action on molten metal droplet transfer during welding and also due to arc rotation the heat will be distributed from the weld joint, so the cooling rate will increase. The spin arc welding technology is developed for welding higher thickness plates without edge preparation. So, edge preparation time and cost will be reduced. Moreover, the number of passes is also minimized; hence the influence of thermal cycles on welded joints is greatly reduced. Due to less number of passes and square butt joint configuration helps to greatly improve the productivity. Based on the previous research works, it is clear that only a few studies on spin arc welding of carbon steel plates have been conducted. However, there is currently no research work on welding of HSLA steel plates using the spin arc welding method. Hence, in this work was to carry out the comparative analysis of mechanical properties and microstructural characteristics of the joints fabricated by spin arc gas welding (SAW) and conventional gas metal arc welding (GMAW) processes. Also correlate the mechanical properties with correspondent microstructural features.

The base metal (BM) used in this investigation is naval grade (DMR249-A) HSLA steel plate of 12 mm thickness. Rolled plates of thick steel were cut to the required dimensions (300x150x12 mm^3) by an abrasive cutting machine. The plates were edge prepared in "V" groove joint design for welding using GMAW (gas metal arc welding) process. Square joint design was prepared for welding using the SAW (Spin arc welding) process (**Fig. 28**). The ER8028 (1.2 mm) filler wire was used to fabricate the joints. The welded joints were cut and machined to the required dimensions for preparing tensile and impact toughness specimens corresponding to American Society for Testing of Materials (ASTM) guidelines. Microstructural examination of the weldments was performed following the procedure prescribed by ASTM E354 standard using a light optical microscope (OM).

The macrographs exhibit that the weld metal (WM) region has very sound joints with no sagging defects, porosity and cracks (**Fig. 29**). The WM area of the GMAW joint is 128.6 mm^2 and the WM area of the SAW joint is 93 mm^2. When comparing the SAW joint to the GMAW joint, the WM area is reduced dramatically (48%). Furthermore, the HAZ width was reduced from 4.40 mm to 2.10 mm, which is a significant benefit of the SAW process. The SAW joint exhibited higher tensile strength

(679 MPa) compared to base metal (614 MPa) and SA-GMAW (515 MPa) joint (**Fig. 30 & 31**). The main important factors being weld metal microstructure and weld metal hardness. The average weld metal hardness of SAW joint is 333 HV but GMAW joint showed 285 HV (**Fig. 32**). When compared to a SAW joint, the weld metal hardness is reduced by 18%. The difference in hardness is caused by the formation of different microstructures, variations in grain size, and the chemical composition of the weld metal. The microstructure of the SAW joint weld metal region is mostly fine acicular ferrite and very fine pearlite, with some bainite microstructure. The GMAW joint is mostly polygonal pearlite with a small amount of acicular ferrite. Higher hardness is due to the fine acicular ferrite microstructure in SAW weld metal. The variations in cooling rates of the welding processes cause the formation of these distinctiveness and different microstructures.

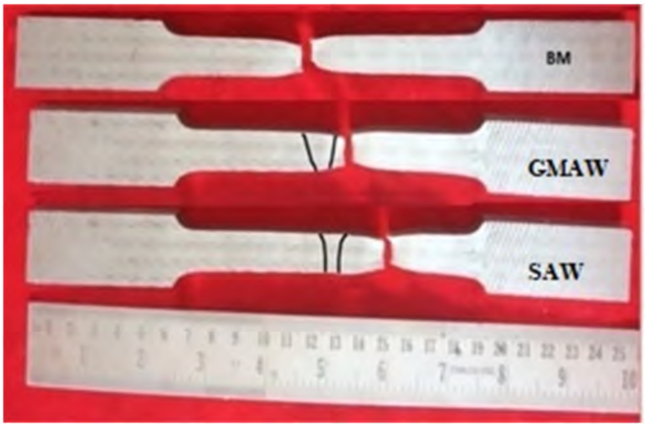

Fig. 30 : Photographs of Tensile Test Specimen

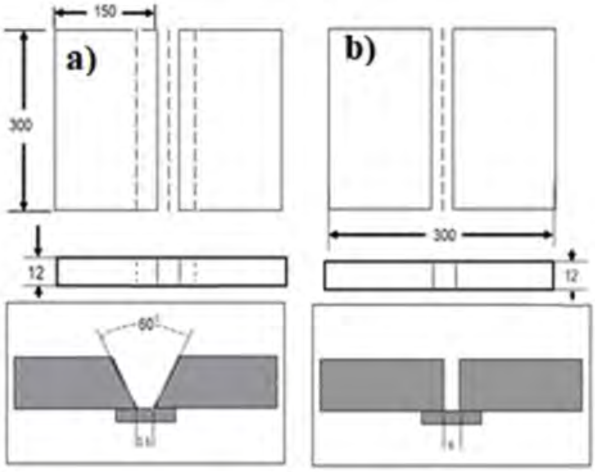

Fig. 28 : Weld Joint Configuration (a) GMAW joint (b) SAW joint.

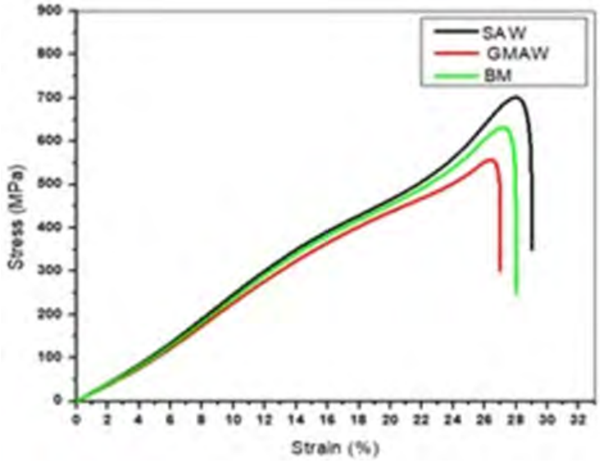

Fig. 31 : Stress – Strain curves for the base metal and welded joints

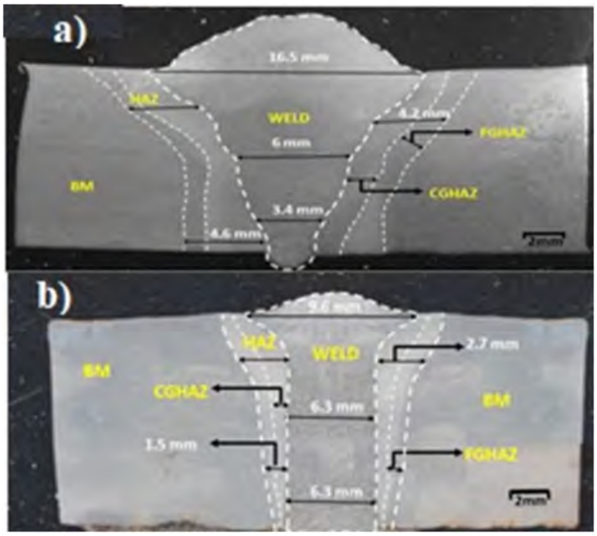

Fig.29 : Macrostructure (a)GMAW joint (b) SAW joint.

The SAW process heat density is distributed more widely during arc rotation, which is influenced by the arc rotation diameter. As a result, heat density at the center of the weld pool is greatly reduced when compared to stationary arc welding processes. As a result, the rotating arc welding process has a lower heat input (3.93 kJ/mm) than the GMAW process (8.41 kJ/mm). The different heat inputs have an effect on the cooling rate. Lower heat input (rapid cooling rate) results in the formation of fine acicular ferrite microstructures in the SAW weld metal region. Because there is no time for grain coarsening, the grain solidifies faster. The cooling rate of in weld metal will be slower if the heat input is higher. This leads to the formation of coarse polygonal ferrite matrix in GMAW joint weld metal region. Lower cooling rate and higher volume percentage of acicular ferrite is the main reasons for higher hardness and tensile strength of spin welding process.

Table 9 : Tensile and Impact toughness properties of welded joints

Joint	0.2% Yield strength (MPa)	Ultimate tensile strength (MPa)	Elongation in 50mm gauge length (%)	Notch tensile strength (MPa)	Notch strength ratio (NSR)	Joint efficiency (%)	Failure location	Impact toughness @ RT (J)
BM	485±6	614±4	28±2	654±6	1.05	-	-	208±7
GMAW	478±3	515±7	27±3	609±8	1.18	83±4	HAZ	247±8
SAW	542±9	679±7	29±2	746±6	1.09	110±2	BM	278±6

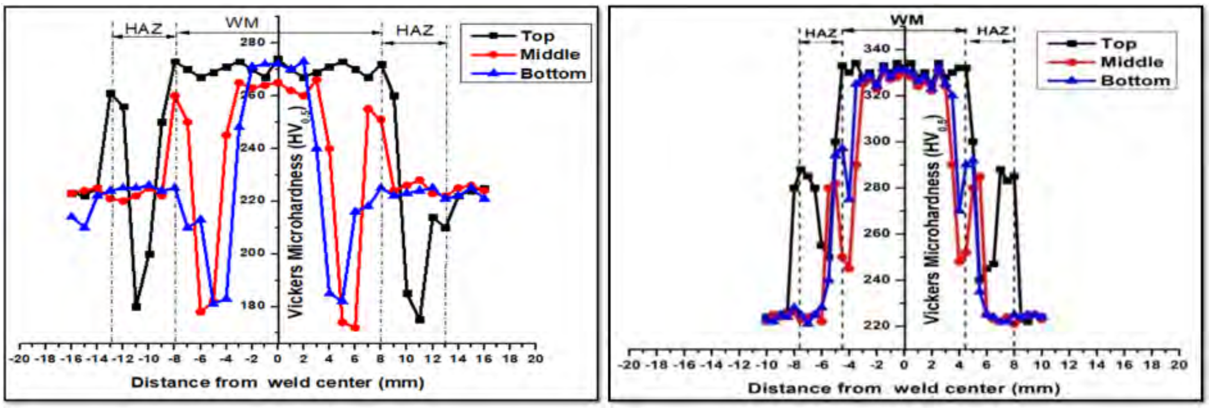

Fig. 32 : Microhardness variation across the welded jointsa) GMAW joint b) SAW joint.

Table 10 : Chemical composition (wt%) of diluted weld metal

Joint	C	Si	Mn	P	S	Cr	Mo	Ni	Al	Cu	Ti	Fe
GMAW	0.022	0.146	1.17	0.006	0.008	0.089	0.014	2.25	0.014	0.169	0.026	Bal
SAW	0.027	0.152	1.26	0.006	0.007	1.08	0.013	2.54	0.014	0.171	0.028	Bal

The impact toughness properties of the base metal and welded joints are shown in **Table 9**. It was inferred that the impact toughness of the SAW joint is greater (278 J) than that of the GMAW joint (247 J) and the base metal (208 J). The impact toughness of the SAW joint was 27 % higher than that of the base metal and the SA-GMAW joint. This is due to four major factors: higher acicular ferrite volume percentage, higher nickel percentage, smaller size inclusions, and fine grain size in the weld metal region. The higher the volume percentage of acicular ferrite (38%), the greater the impact toughness.

The acicular ferrite structure with needle shape morphology prevents the development the formation of a crack in the weld metal. **Fig.33 (a)** shows polygonal ferrite microstructure in the weld metal region. The polygonal ferrite microstructure is having low impact toughness when compared to the acicular ferrite microstructure, so the cracks will develop easily along the polygonal ferrite grain boundaries. The acicular ferrite microstructure is the favourable structure for increasing toughness on the SAW joint **Fig. 33 (b)**. **Table 10** shows the chemical composition (in weight present) of the diluted elements in both weld metals. It is understood that the Ni and Mn weight percentages vary significantly in the GMAW process. Furthermore, the GMAW joint had a lower nickel percentage. This could be one of the factors contributing to the reduction of impact toughness properties in the GMA weld metal region. The Ni and Mn elements are 10 % and 6 % lower than in the SAW joint. Higher weight percentage Ni and Mn in the weld metal are responsible for improved impact toughness properties. Therefore, it can be concluded that the WM microstructure and inclusion content are the reasons for the huge variation in impact toughness properties of both GMAW and SAW joints.

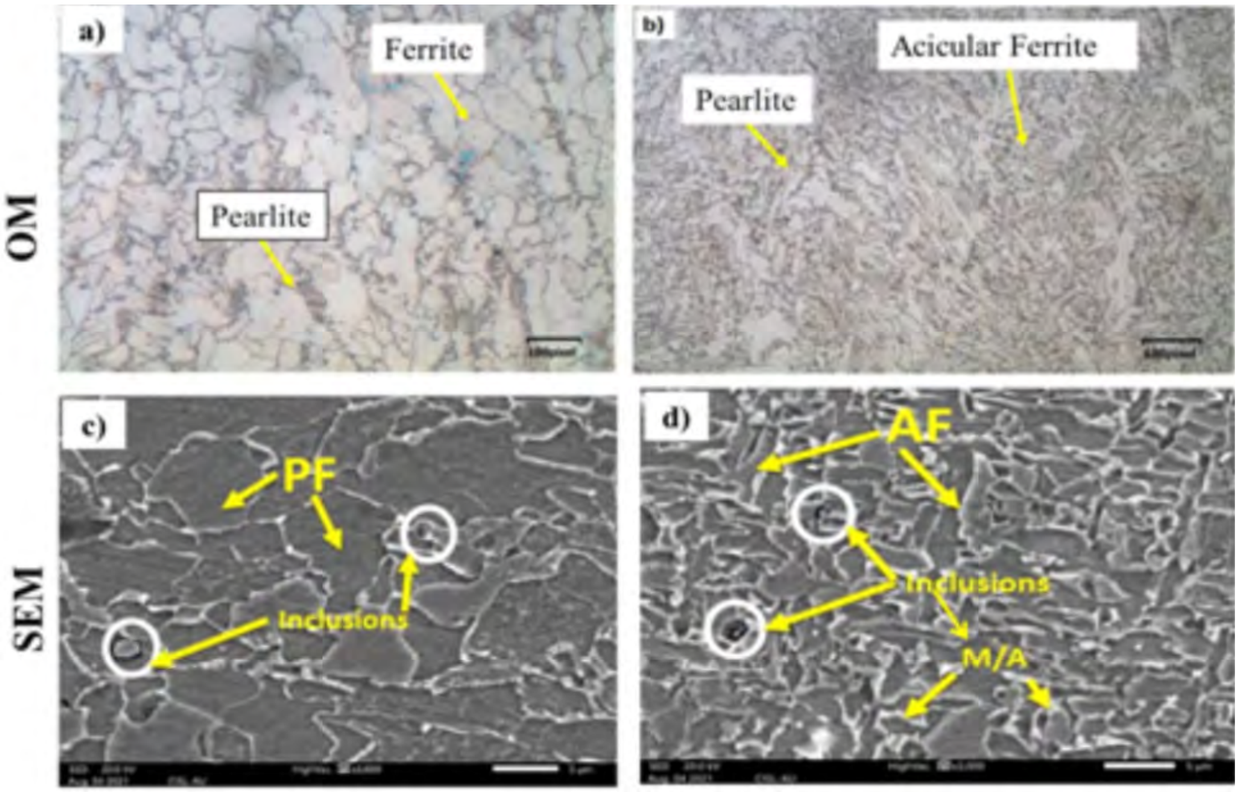

Fig. 33 : OM and SEM images of weld metal (WM) region a, c) GMAW joint b, d) SAW joint PF-Polygonal Ferrite, AF-Acicular Ferrite, M/A-martensite and austenite islands

The SAW joints have better tensile strength and weld metal hardness than GMAW joints. Moreover, the SAW joint had a 15% higher joint efficiency than the GMAW joint. This is because the weld metal region contains a higher volume percentage of fine acicular ferrite mixed with fine pearlite.

The SAW joint has 15% greater ductility and impact toughness than the GMAW joint. This is due to the presence of more large-sized inclusions and coarse grains in the GMAW joint weld metal.

6.0 Wire Arc Additive Manufacturing of Aluminum Alloy Components

With the advancement of industry, the requirements for high efficiency, lightweight, and low cost are becoming more demanding. Additive manufacturing (AM) technology is a novel method of producing near net-shaped metallic components with complicated geometry at a reasonable cost. Metal additive manufacturing is a technology that has received a lot of attention in recent years. Metal additive manufacturing is more efficient and produces more complex geometrical components than traditional manufacturing processes like casting, forging, or welding. WAAM is probably one of the most potential techniques among the different metal AM methods for producing large components, due to its very high deposition rate compared with other processes based on heat sources of the laser or electron beam [1].

WAAM is a potential technique for producing large components of aluminium. In WAAM, various welding defects like hot cracks and porosity can occur in aluminum alloys. Porosity is generated for various reasons, such as arc welding, process parameters like high current and voltage, quality of wire, alloying elements, and interpass temperature. The heat input of a new superimposed layer can promote the development of pores in a multi-layer WAAM process. However, Mg is a very active element and the Al–Mg alloy is highly heat-sensitive (prone to porosity). Aside from hot cracking, porosity in WAAM of aluminium alloys is a major issue that severely limits the mechanical properties of the part [2]. Therefore, a suitable WAAM method must be selected to manufacture large aluminum parts that possess better properties. From the published data, it is conceived that most of the research was done on the WAAM of microstructure and mechanical properties of linear wall aluminum components. There is no documentation on the effect of welding processes on the porosity and microstructural and mechanical properties of WAAM AA5356 aluminum alloy cylindrical components. Therefore, the need for an effective welding process, control, and monitoring system is essential. The motivation behind the current study is to compare the GMAW and CMT processes for homogeneous microstructure and isotropic mechanical properties of WAAMAA5356 aluminum alloy cylindrical components. The effect of heat input on microstructural features and mechanical properties was studied in different zones of GMAW- and CMT-based AA5356 aluminum alloy cylindrical components.

Table 11 shows the chemical composition of the ER5356 (Al-Mg) filler wire (Φ = 1.2 mm) used in this study. The additively manufactured cylindrical components were built with a welding machine (CMT Advanced 4000 R), capable of working on the GMAW and CMT variants. The three axes automatic motion of the welding torch arrangement made with welding machine with the rotating table. **Table 12** shows the optimized process parameters for GMAW and CMTAW processes. Before deposition, the aluminum 6061 (250 × 250 × 10 mm) substrate was cleaned, and the arc torch kept constant perpendicular to the surface of the substrate during deposition. Meanwhile, the substrate will rotate with the arrangement of a mechanical motor system. The lower and upper zones of the manufactured Al-Mg cylindrical components were separated, and a computer numerical control (CNC) lath machine was used to remove excessive material, as shown in **Fig. 34** with a 4-mm wall thickness. The influence of heat input on microstructure was examined at various regions of the cylindrical components. There has also been an analysis of changes in microstructural characteristics and phases at different regions of the cylindrical components. In addition, the tensile properties, hardness and impact toughness of the GMAW and CMT produced cylindrical components have been studied to assess compatibility of the WAAM components with real time applications.

Table 13 presents the percentage of porosity, average pore size, number of pores, and total porous area of the Al-Mg alloy components. The pores with a diameter greater than 10 μm are measured in the components. As can be seen in **Fig. 35**, the GMAW component has a large number and size of pores. The number of pores and pore size were lower, and the percentage of porosity was reduced in the CMT component.

Table 11 : Chemical composition (wt %) of ER5356 filler wire

Wire	Si	Cu	Fe	Mn	Mg	Cr	Zn	Ti	Be	Al
ER5356	0.25	0.1	0.4	0.07	4.5	0.06	0.1	0.06	0.0003	Bal.

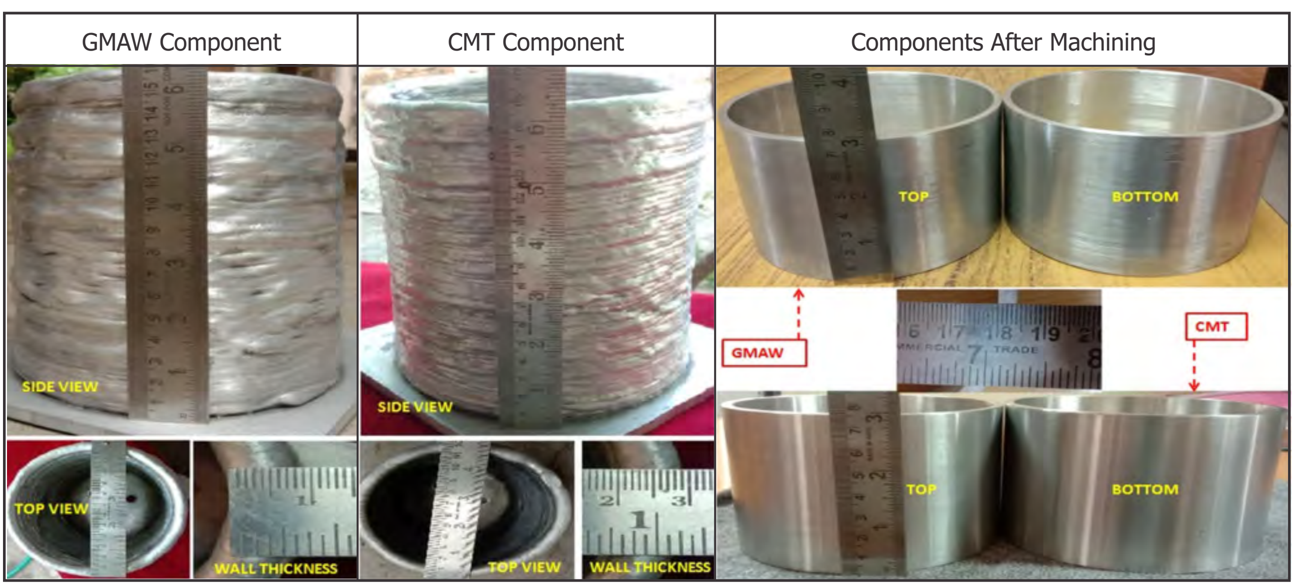

Fig. 34 : Photographs of manufactured cylindrical components (before and after machining)

Table 12 : Optimized WAAM process parameters

Wire feed speed (m/min)	6.4	6.4
Current (A)	121	105
Voltage (v)	13.5	13.0
Travel speed (mm/min)	250	250
Arc length correction (%)	----	0
100% Ar (lit/min)	18	18

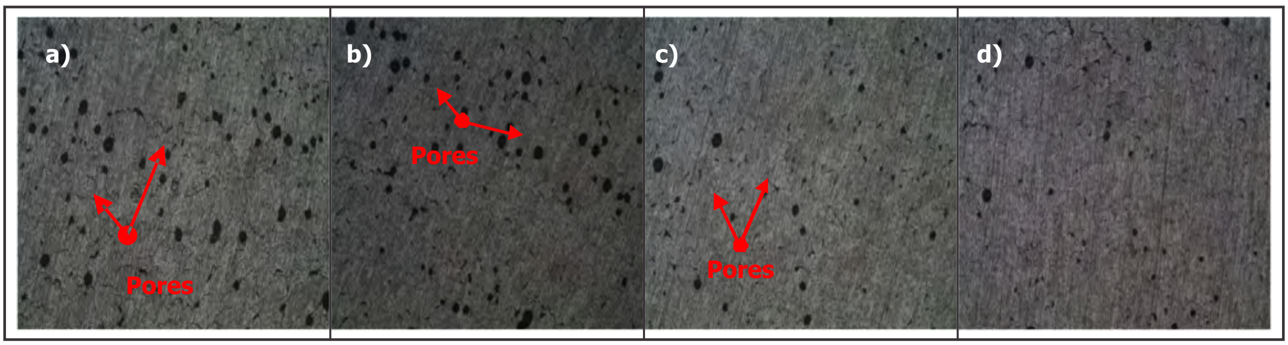

Fig. 35 : Distribution of pores in the lower and upper zones: (a, b) GMAW and (c, d) CMT

Table 13 : Porosity analysis

Process	Location	Number of pores	Total porous area (mm^2)	Pore diameter (μm)	Percentage porosity (%)
GMAW	Lower	68	1.360	96.75	2.60
	Upper	60	1.248	86.93	2.30
CMT	Lower	31	0.577	57.89	0.90
	Upper	20	0.357	47.73	0.68

Fig. 36 shows the standard stress versus strain curves and microhardness distribution for the lower and upper zones of the cylindrical components of aluminum alloy. **Table 14** additionally presents the lower and upper zones of the mechanical properties of WAAM Al-Mg cylinders. The mechanical properties (YS, UTS, elongation hardness and impact toughness) were slightly changed from the lower to the upper zone of the GMAW cylindrical component.

Similar differences in tensile properties of WAAM aluminum parts were observed in recent studies [3, 4]. The mechanical properties of the GMAW Al-Mg alloy component vary from the lower to the upper zone due to differences in microstructural features and pores distribution. The NSR values are above one, which proves that the fabricated components are notch ductile in nature. The microhardness and impact toughness of the lower and upper zones of the GMAW component appreciably varied.

Table 14 : Mechanical properties of WAAM AA5356 aluminum alloy cylindrical components

Process	Sample	UTS (MPa)	0.2% Y.S (MPa)	Elongation (%)	NTS (MPa)	NSR (%)	Impact Toughness at RT (J)	Average Hardness ($HV_{0.5}$)	Heat Input (kJ/mm)
GMAW	Lower	215	121	35.80	242	1.12	9	67.18	0.313
	Upper	224	135	41.20	244	1.08	11	72.70	
CMT	Lower	254	161	46.93	261	1.02	13	83.34	0.262
	Upper	258	168	49.20	276	1.06	14	85.86	

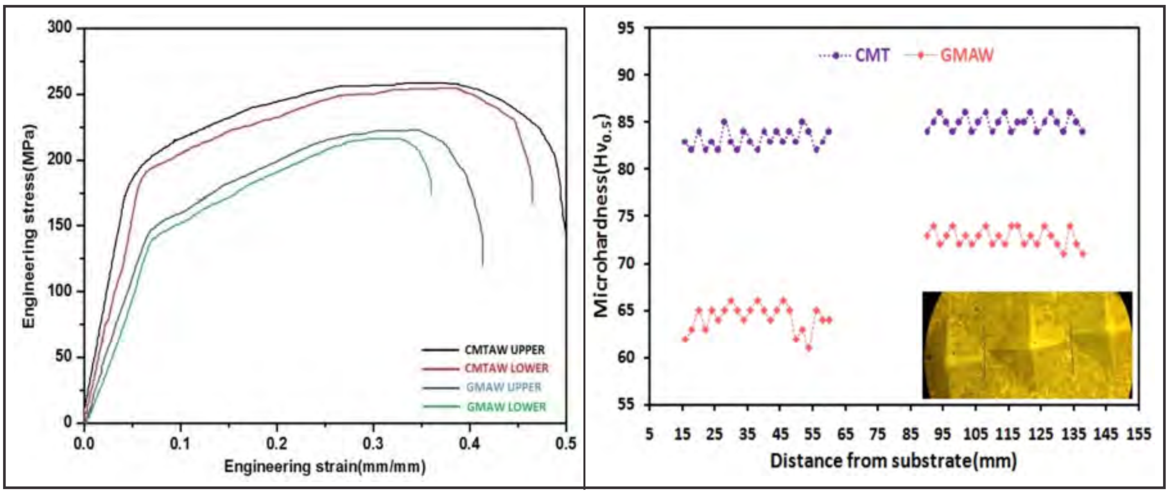

Fig. 36 : Mechanical properties of cylindrical components: a) Stress vs Strain curve and b) Microhardness distribution

The CMT Al-Mg alloy cylinder showed isotropic mechanical properties (YS, UTS, elongation hardness, and impact toughness) in both zones, indicating isotropic behavior in mechanical properties. The uniform microstructural features with reduced segregation of secondary phases (β) in the deposited layers are the main reason for isotropic mechanical properties of the CMT cylinder. Similar isotropy in mechanical properties of WAAM aluminum parts were observed in recent investigations [2, 5].

The specimens extracted from the lower and upper zones of the CMT component exhibited higher strength (UTS, YS), hardness, and toughness than the GMAW component due to the formation of an equiaxed microstructure with reduced porosity. The secondary phase (β) will segregate at grain boundaries when the magnesium content is more than 3 wt. % due to the lower solubility of magnesium (1.9 wt.%) in aluminum at room temperature. The segregation of these (β) phases will affect the mechanical properties of WAAM parts. CMT is a variant of GMAW; it is a novel method for WAAM. It uses a mechanism for wire retraction that delivers signal that retracts filler wire and offers weld time to cool back each drop. The wire moves continuously until the short circuit takes place in the CMT process. The following structural changes were identified due to the low heat input of the CMT process: (i) because of the fast cooling due to low heat input, the CMT component produced a finer grain size than the GMAW cylindrical component. From the SEM with EDS analysis (shown in Fig.4), it is confirmed that the element magnesium did not precipitate in time, and the maximum amount of magnesium dissolved in the α-Al matrix. Al-Mg alloy cylindrical component manufactured by CMT WAAM produced a fine primary α-Al phase that acted as fine grain strengthening, as well as changed the structure of the segregated phase, which improved the mechanical properties of the component.

The Al-Mg cylindrical component manufactured by CMT process showed almost equal values of tensile properties, hardness, and impact toughness in both zones, indicating isotropic behavior of mechanical properties. Moreover, grain size is finer, and the segregated β-(Al_3Mg_2) phases are lower and thinner, and the solid solution of magnesium increased in

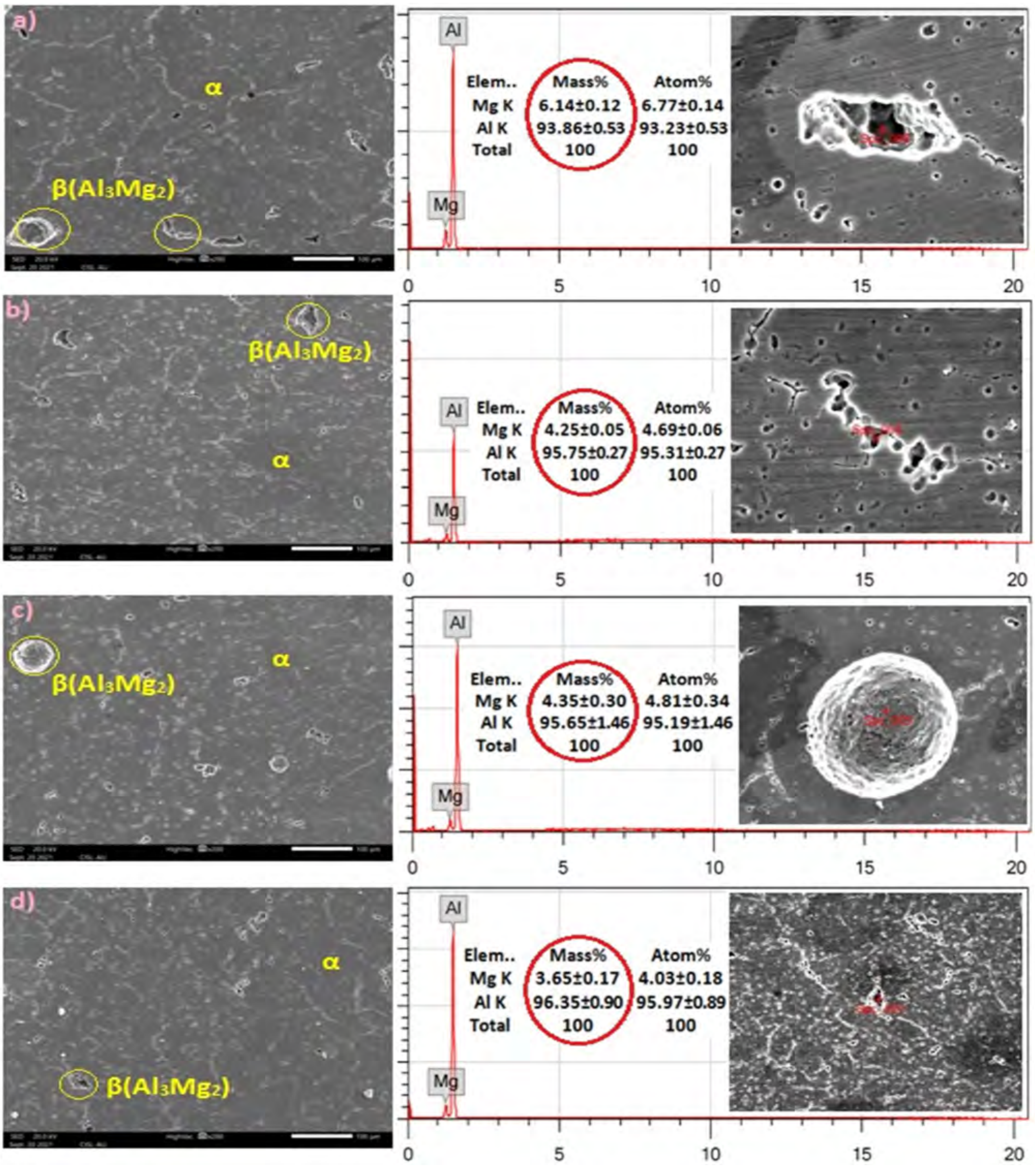

Fig.37 : SEM and EDS photographs of lower and upper zones cylindrical components: (a, c) GMAW, and (b, d) CMT

aluminum, which increased the solid solution strengthening effect in the cylinder.

Acknowledgements:

The author wish to record sincere thanks to his colleagues, research scholars and funding agencies for carrying out these advanced researches in Centre for Materials Joining & Research (CEMAJOR), Annamalai University, Annamalainagar, Chidambaram, Tamilnadu (which is located in a socially, economically and industrially disadvantaged rural town).

(i) Dr. S. Malarvizhi, Professor, CEMAJOR;

(ii) Dr. K. Shanmugam, Professor, CEMAJOR;

(iii) Dr. K. Srinivasan, Associate Professor, CEMAJOR;

(iv) Dr. S. Rajakumar, Associate Professor, CEMAJOR;

(v) Dr. P. Sivaraj, Associate Professor, CEMAJOR;

(vi) Dr. C. Rajendran, Research Scholar, CEMAJOR (FSW Process);

(vii) Dr. Arun Negamiya, Research Scholar, CEMAJOR (DB Process);

(viii) Mr. C. Mukundan, Research Scholars, CEMAJOR (LFW Process);

(ix) Dr. Tushar Sonar, Research Scholar, CEMAJOR (GTCAW Process);

(x) Mr. N. Sankar, Research Scholar, CEMAJOR (RA-GMAW Process);

(xi) Mr. Nagasai Prasanna, Research Scholar, CEMAJOR (WAAM Process);

Aeronautical Development Agency (ADA), Bangalore for FSW research, University Grants Commission (UGC), New Delhi for DB research, Gas Turbine Research & Establishment (GTRE), DRDO, Bangalore for LFW research, Vikram Sarabhai Space Centre (VSSC), ISRO, Trivandrum for GTCAW research, Combat Vehicles Research & Development Establishment (CVRDE), DRDO, Avadi, Chennai for RA-GMAW research and M/s. Fronius India Private Limited, Chennai for WAAM research.